



CHORUS

This is the accepted manuscript made available via CHORUS. The article has been published as:

Total absorption γ -ray spectroscopy of the β -delayed neutron emitters ^{87}Br , ^{88}Br , and ^{94}Rb

E. Valencia *et al.*

Phys. Rev. C **95**, 024320 — Published 21 February 2017

DOI: [10.1103/PhysRevC.95.024320](https://doi.org/10.1103/PhysRevC.95.024320)

Total Absorption γ -Ray Spectroscopy of ^{87}Br , ^{88}Br and ^{94}Rb β -Delayed Neutron Emitters

E. Valencia, J. L. Tain,* A. Algora,† J. Agramunt, E. Estevez, M.D. Jordan, and B. Rubio
Instituto de Fisica Corpuscular (CSIC-Universitat de Valencia), Apdo. Correos 22085, E-46071 Valencia, Spain

S. Rice, P. Regan, W. Gelletly, Z. Podolyák, M. Bowry, P. Mason, and G. F. Farrelly
University of Surrey, Department of Physics, Guilford GU2 7XH, United Kingdom

A. Zakari-Issoufou, M. Fallot, A. Porta, and V. M. Bui
SUBATECH, CNRS/IN2P3, Universit de Nantes, Ecole des Mines, F-44307 Nantes, France

J. Rissanen, T. Eronen, I. Moore, H. Penttilä, J. Äystö, V.-V. Elomaa, J. Hakala, A. Jokinen, V. S. Kolhinen, M. Reponen, and V. Sonnenschein
University of Jyväskylä, Department of Physics, P.O. Box 35, FI-40014 University of Jyväskylä, Finland

D. Cano-Ott, A. R. Garcia, T. Martínez, and E. Mendoza
Centro de Investigaciones Energéticas Medioambientales y Tecnológicas, E-28040 Madrid, Spain

R. Caballero-Folch, B. Gomez-Hornillos, and V. Gorlichev
Universitat Politècnica de Catalunya, E-08028 Barcelona, Spain

F. G. Kondev
Nuclear Engineering Division, Argonne National Laboratory, Argonne, Illinois 60439, USA

A. A. Sonzogni
NNDC, Brookhaven National Laboratory, Upton, New York 11973, USA

L. Batist
Petersburg Nuclear Physics Institute, Gatchina, Russia
(Dated: January 24, 2017)

We investigate the decay of $^{87,88}\text{Br}$ and ^{94}Rb using total absorption γ -ray spectroscopy. These important fission products are β -delayed neutron emitters. Our data show considerable $\beta\gamma$ -intensity, so far unobserved in high-resolution γ -ray spectroscopy, from states at high excitation energy. We also find significant differences with the β intensity that can be deduced from existing measurements of the β spectrum. We evaluate the impact of the present data on reactor decay heat using summation calculations. Although the effect is relatively small it helps to reduce the discrepancy between calculations and integral measurements of the photon component for ^{235}U fission at cooling times in the range 1 – 100 s. We also use summation calculations to evaluate the impact of present data on reactor antineutrino spectra. We find a significant effect at antineutrino energies in the range of 5 to 9 MeV. In addition, we observe an unexpected strong probability for γ emission from neutron unbound states populated in the daughter nucleus. The γ branching is compared to Hauser-Feshbach calculations which allow one to explain the large value for bromine isotopes as due to nuclear structure. However the branching for ^{94}Rb , although much smaller, hints of the need to increase the radiative width Γ_γ by one order-of-magnitude. This increase in Γ_γ would lead to a similar increase in the calculated (n, γ) cross section for this very neutron-rich nucleus with a potential impact on r process abundance calculations.

I. INTRODUCTION

Total absorption gamma-ray spectroscopy (TAGS) has been applied to study the decay of three fission products (FP) which are β -delayed neutron emitters. We present

in this work the results of this study and discuss the impact on three research topics of current interest: 1) reactor decay heat (DH) calculations, 2) reactor antineutrino $\bar{\nu}_e$ spectrum calculations, and 3) the study of the emission of γ -rays from neutron-unbound states and its relation to neutron capture (n, γ) reactions.

The isotopes included in the present study are ^{87}Br , ^{88}Br and ^{94}Rb . These are neutron-rich nuclei with relatively short half-life $T_{1/2}$, large decay energy window Q_β , large neutron separation energy S_n in the daughter

* Corresponding author: tain@ific.uv.es

† Institute of Nuclear Research of the Hungarian Academy of Sciences, H-4026 Debrecen, Hungary

37 nucleus, and moderate neutron emission probability P_n
 38 as can be observed in Table I, showing decay parameters
 39 taken from the ENSDF data base [1–3].

TABLE I. Half-life $T_{1/2}$, neutron emission probability P_n , decay energy window Q_β , and daughter neutron separation energy S_n for each measured isotope. Values taken from Ref. [1–3].

Isotope	$T_{1/2}$ (s)	P_n (%)	Q_β (MeV)	S_n (MeV)
^{87}Br	55.65(13)	2.60(4)	6.852(18)	5.515(1)
^{88}Br	16.34(8)	6.58(18)	8.975(4)	7.054(3)
^{94}Rb	2.702(5)	10.18(24)	10.281(8)	6.828(10)

40 The three aforementioned topics of research benefit
 41 from the application of the TAGS technique to obtain
 42 the β intensity distribution of decays followed by γ -ray
 43 emission. States at high excitation energy in the daughter
 44 nucleus can be populated if Q_β is large. In this case
 45 both the number of levels over which the β intensity is
 46 distributed and the number of levels available for γ de-
 47 excitation is large. Thus individual γ -rays collect little
 48 intensity and the use of high resolution gamma-ray
 49 spectroscopy (HRGS) with germanium detectors typically
 50 fails to detect some of them. This problem has
 51 come to be known as the *Pandemonium* effect [4]. As a
 52 consequence β intensity distributions determined from γ -
 53 ray intensity balance tend to be distorted with an excess
 54 of β intensity assigned at low excitation energies. The
 55 TAGS technique [5], using large 4π scintillation detectors,
 56 is based on the detection of the full de-excitation
 57 cascade, rather than individual γ -rays, and thus over-
 58 comes the *Pandemonium* effect. The power of the TAGS
 59 method to locate the missing β intensity has been demon-
 60 strated before [6–8]. The distortion of the β -intensity dis-
 61 tributions obtained from HRGS causes a systematic error
 62 in the calculated average β and γ decay energies. This
 63 affects the calculation of the DH time evolution using
 64 the summation method, which relies on decay data from
 65 individual precursors. Similarly the distortion of the β
 66 intensity affects the calculated spectrum of antineutrinos
 67 emitted from reactors using the summation method.
 68 *Pandemonium* also prevents the correct determination of
 69 the gamma-to-neutron emission ratios from states popu-
 70 lated above S_n in the daughter nucleus.

71 Subsections IA, IB and IC of this Section provide
 72 background information on the three research topics, detail
 73 the influence of *Pandemonium* for each of them, and
 74 points out the relevance of the selected isotopes. The
 75 remainder of the paper is organized as follows. Details
 76 of the experimental method are given in Section II. The
 77 analysis of the data, the β intensity distributions and the
 78 evaluation of uncertainties are presented in Section III.
 79 The impact of the average β and γ decay energies de-
 80 termined in this work on DH calculations is presented in

81 Section IV. The effect on calculated antineutrino spectra
 82 is shown in Section V. The evaluation of γ to neutron
 83 branching ratios is presented in Section IV and compared
 84 with Hauser-Feshbach calculations in Section VII
 85 together with a discussion of the possible impact on neu-
 86 tron capture cross section estimates for unstable very
 87 neutron-rich nuclei. Partial results of the work presented
 88 here were already published in Ref. [9].

89 A. Reactor decay heat

90 A knowledge of the heating produced by radioactive
 91 products in a reactor and its time evolution after reactor
 92 shutdown is important for reactor safety. In conventional
 93 reactors the DH is dominated by FP for cooling times up
 94 to a few years. An issue in reactor DH studies has been
 95 the persistent failure of summation calculations to re-
 96 produce the results of integral experiments for individual
 97 fissioning systems. Summation calculations are based on
 98 individual FP yields and average γ -ray and β energies
 99 retrieved from evaluated nuclear data bases. In spite of
 100 this deficiency summation calculations remain an impor-
 101 tant tool in reactor safety studies. For example, after the
 102 Fukushima Dai-ichi nuclear plant accident it was pointed
 103 out [10] that summation calculations are relevant to un-
 104 derstand the progression of core meltdown in this type of
 105 event. The Fukushima accident was the consequence of a
 106 failure to dissipate effectively the DH in the reactor core
 107 and in the adjacent spent fuel cooling pool. Summation
 108 calculations are particularly important in design studies
 109 of innovative reactor systems (Gen IV reactors, Accel-
 110 erator Driven Systems) with unusual fuel compositions
 111 (large fraction of minor actinides), high burn ups and/or
 112 harder neutron spectra, since integral data are missing.

113 Yoshida and Nakasima [11] recognized that the
 114 *Pandemonium* systematic error is responsible for a sub-
 115 stantial fraction of the discrepancy between DH integral
 116 experiments and calculations. The average γ and β en-
 117 ergy for each isotope, \bar{E}_γ and \bar{E}_β respectively, can be
 118 computed from $I_\beta(E_x)$, the β intensity distribution as a
 119 function of excitation energy E_x as

$$\bar{E}_\gamma = \int_0^{Q_\beta} I_\beta(E_x) E_x dE_x \quad (1)$$

$$\bar{E}_\beta = \int_0^{Q_\beta} I_\beta(E_x) \langle E_\beta(Q_\beta - E_x) \rangle dE_x \quad (2)$$

120 Here $\langle E_\beta(Q_\beta - E_x) \rangle$ represents the mean value of the β
 121 energy continuum leading to a state at E_x . According to
 122 Eq. 1 and 2, the *Pandemonium* systematic error affecting
 123 HRGS data has the effect of artificially decreasing the
 124 average γ -ray energy and increasing the average β energy.
 125 The TAGS technique, free from *Pandemonium*, was
 126 applied in the 1990s by Greenwood and collaborators at
 127 INEL (Idaho) [12] to obtain accurate average decay en-
 128 ergies for up to 48 FP with impact in DH calculations.

129 Recognizing the importance of this approach to improv-
 130 ing summation calculations, the OECD/NEA Working
 131 Party on International Evaluation Cooperation (WPEC)
 132 established subgroup SG25 to review the situation [13].
 133 Recommendations were made, in the form of priority
 134 lists, for future TAGS measurements on specific isotopes
 135 for the U/Pu fuel cycle. The work was later extended
 136 to the Th/U fuel cycle by Nichols and collaborators [14].
 137 The results of Algora *et al.* [15] demonstrated the large
 138 impact of new TAGS measurements for a few isotopes
 139 selected from the priority list.

140 From the nuclei included in the present work ^{87}Br was
 141 assigned priority 1 in Ref. [13, 14] for a TAGS mea-
 142 surement, although it is an example of a well studied
 143 level scheme [1] with up to 374 γ transitions de-exciting
 144 181 levels. The justification for the high priority comes
 145 from: 1) the large uncertainty (25%) on average ener-
 146 gies coming from the spread of intensity normalization
 147 values between different measurements, 2) a potential
 148 *Pandemonium* error suggested by the number of ob-
 149 served levels at high excitation energies (less than half
 150 of the expected number according to level density esti-
 151 mates) and 3) the large contribution to DH around 100 s
 152 cooling time. ^{88}Br also has priority 1 in Ref. [13, 14].
 153 It contributes significantly to the DH at cooling times
 154 around 10 s. The known decay scheme [2] is rather in-
 155 complete above $E_x = 3.5$ MeV, from level density con-
 156 siderations, as shown in the RIPL-3 reference input pa-
 157 rameter library web page [16]. We estimate that more
 158 than 300 levels should be populated in the decay above
 159 $E_x = 3.5$ MeV and below S_n in comparison with the ob-
 160 served number of 33. ^{94}Rb is not included in the priority
 161 list of Ref. [13] but is considered to be of relative impor-
 162 tance in Refs. [14] and [17] for short cooling times. The
 163 decay scheme is very poorly known [3]. Only 37 levels
 164 are identified above $E_x = 3.4$ MeV, regarded as the max-
 165 imum energy with a complete level scheme [16]. We esti-
 166 mate that more than 900 levels could be populated below
 167 S_n thus pointing to a potentially strong *Pandemonium*
 168 effect.

169 B. Reactor antineutrino spectrum

170 An accurate knowledge of the reactor anti-neutrino $\bar{\nu}_e$
 171 spectrum is of relevance for the analysis of neutrino oscil-
 172 lation experiments [18, 19] and for exploring the use of
 173 compact anti-neutrino detectors in nuclear proliferation
 174 control [20]. Summation calculations are also a valuable
 175 tool to obtain the $\bar{\nu}_e$ spectrum but suffer from the same
 176 problem as DH summation calculations: inaccuracies in
 177 fission yields and individual precursor decay data.

178 For each fission product the electron antineutrino spec-
 179 trum $S_{\bar{\nu}}(E_{\bar{\nu}})$, and the related β spectrum $S_{\beta}(E_{\beta})$, can be
 180 computed from the β intensity distribution

$$S_{\bar{\nu}}(E_{\bar{\nu}}) = \int_0^{Q_{\beta}} I_{\beta}(E_x) s_{\bar{\nu}}(Q_{\beta} - E_x, E_{\bar{\nu}}) dE_x \quad (3)$$

$$S_{\beta}(E_{\beta}) = \int_0^{Q_{\beta}} I_{\beta}(E_x) s_{\beta}(Q_{\beta} - E_x, E_{\beta}) dE_x \quad (4)$$

181 where $s_{\bar{\nu}}(Q_{\beta} - E_x, E_{\bar{\nu}})$ and $s_{\beta}(Q_{\beta} - E_x, E_{\beta})$ represent
 182 the shape of $\bar{\nu}_e$ and β energy distributions for the transi-
 183 tion to a state at E_x . For each E_x , $s_{\bar{\nu}}$ and s_{β} are related
 184 by energy-conservation $E_{\bar{\nu}} = Q_{\beta} - E_x - E_{\beta}$ to a good
 185 approximation. Thus distortions of the observed $I_{\beta}(E_x)$
 186 distribution in HRGS due to *Pandemonium* tend to pro-
 187 duce calculated $\bar{\nu}_e$ spectra shifted to higher energies.

188 Currently the most reliable reactor $\bar{\nu}_e$ spectra are ob-
 189 tained from integral β -spectrum measurements of ^{235}U ,
 190 ^{239}Pu and ^{241}Pu thermal fission performed by Schreck-
 191 enbach *et al.* at ILL-Grenoble [21, 22]. Data on ^{238}U
 192 fast fission also became available recently [23]. The con-
 193 version of integral β spectra to $\bar{\nu}_e$ spectra requires a
 194 number of approximations. These are needed because,
 195 as pointed out above, the transformation is isotope and
 196 level dependent. The global conversion procedure has
 197 been revised and improved recently [24, 25]. As a conse-
 198 quence of this revision a change of normalization in the
 199 detected spectrum is found that contributes to a con-
 200 sistent deficit when comparing $\bar{\nu}_e$ rates from short base
 201 line experiments with calculations [26], a surprising ef-
 202 fect which is termed the reactor neutrino anomaly. The
 203 possibility that the deficit is related to the existence of
 204 sterile neutrinos has aroused considerable interest. On
 205 the other hand, several sources of systematic error could
 206 explain the anomaly. In particular the effect could be re-
 207 lated to an abundance of transitions of the first forbidden
 208 type [27] for which the spectral shape is not well known.
 209 The β spectrum depends in this case on the nuclear wave
 210 functions, departing from the allowed shape. In addition
 211 higher order corrections to the shape, mainly the weak
 212 magnetism correction dependent on transition type, play
 213 a significant role. Nuclear structure calculations [28] also
 214 show the relevance of using the correct β shape for indi-
 215 vidual decay branches. The experimental investigation of
 216 this or similar effects benefits from accurate decay mea-
 217 surements of individual fission products and the use of
 218 the summation method as was argued in [29].

219 The statistics accumulated in the three running reactor
 220 $\bar{\nu}_e$ experiments, Double Chooz [30], RENO [31] and Daya
 221 Bay [32], has revealed differences between the shape of
 222 the calculated $\bar{\nu}_e$ spectra and the measured one. Several
 223 possible sources for the shape distortion have been dis-
 224 cussed [33]. The observed excess between 5 and 7 MeV
 225 $E_{\bar{\nu}_e}$ could be due to the contribution of a few specific
 226 FP [34, 35] which is not reproduced by the global con-
 227 version method. Thus the study of this new antineu-
 228 trino shape distortion requires the use of the summation
 229 method and reinforces the need for new accurate decay
 230 data with the TAGS technique. As a matter of fact one
 231 of the key isotopes in this list, ^{92}Rb , was part of the

232 same experiment analyzed here and its impact on the
 233 antineutrino spectrum was already evaluated [36]. From
 234 the isotopes studied in the present work ^{94}Rb has an ap-
 235 preciable contribution to the high energy part of the $\bar{\nu}_e$
 236 spectrum.

237 Another approach to the improvement of decay data
 238 for both $\bar{\nu}_e$ and DH summation calculations was followed
 239 in the past by Tengblad *et al.* [37]. They measured the
 240 spectrum of electrons emitted in the decay of individ-
 241 ual FP using charged particle telescopes. This method
 242 is in essence *Pandemonium* free. Measurements were
 243 performed for up to 111 fission products at ISOLDE
 244 (Geneva) and OSIRIS (Studsvik). The β spectra are
 245 converted into $\bar{\nu}_e$ spectra and both are tabulated for 95
 246 isotopes in Ref. [38]. It was first pointed out by O. Bersil-
 247 lon during the work of WPEC-SG25 [13] that average β
 248 energies from Tengblad *et al.* [37] can be compared with
 249 average β energies calculated from TAGS data obtained
 250 by Greenwood *et al.* [12] (see also Subsection IA) for up
 251 to 18 fission products. The comparison shows that \bar{E}_β
 252 energies from Tengblad *et al.* are systematically larger
 253 than those from Greenwood *et al.*. The average differ-
 254 ence is +177 keV with a spread of values from -33 keV
 255 to +640 keV. In view of the relevance of both sets of
 256 data it is important to confirm the discrepancy and in-
 257 vestigate possible causes. The list of measured isotopes
 258 in [37, 38] includes $^{87,88}\text{Br}$ and ^{94}Rb thus they can be
 259 compared with our data.

260 C. Gamma-ray emission from neutron unbound 261 states

262 Neutron-unbound states can be populated in the β -
 263 decay of very neutron-rich nuclei, when the neutron sepa-
 264 ration energy S_n in the daughter nucleus is lower than the
 265 decay energy window Q_β . The relative strength of strong
 266 and electromagnetic interactions determines that typi-
 267 cally neutron emission from these states predominates
 268 over γ -ray emission. These emission rates are quantified
 269 by the partial level widths Γ_n and Γ_γ respectively. The
 270 fraction of β intensity followed by γ -ray emission is given
 271 by $\Gamma_\gamma/\Gamma_{tot}$, with $\Gamma_{tot} = \Gamma_\gamma + \Gamma_n$. There is an analogy [39]
 272 between this decay process and neutron capture reac-
 273 tions populating unbound states. Such resonances in the
 274 compound nucleus re-emit a neutron (elastic channel) or
 275 de-excite by γ -rays (radiative capture). Indeed the reac-
 276 tion cross section is parametrized in terms of neutron and
 277 γ widths. In particular the (n, γ) cross section includes
 278 terms proportional to $\Gamma_\gamma\Gamma_n/\Gamma_{tot}$. Notice that the spins
 279 and parities of states populated in β -decay and (n, γ) do
 280 not coincide in general because of the different spin and
 281 parity of the respective parent and target nuclei and the
 282 different selection rules.

283 Neutron capture and transmission reactions have been
 284 extensively used [40] to determine Γ_γ and Γ_n of resolved
 285 resonances, or the related strength functions in the unre-
 286 solved resonance region. An inspection of Ref. [40] shows

287 that in general Γ_n is measured in eV or keV while Γ_γ is
 288 measured in meV or eV, in agreement with expectation.
 289 Current data are restricted, however, to nuclei close to
 290 stability since such experiments require the use of stable
 291 or long-lived targets. On the other hand, (n, γ) capture
 292 cross sections for very neutron-rich nuclei are a key ingre-
 293 dient in reaction network calculations describing the syn-
 294 thesis of elements heavier than iron during the rapid (*r*)
 295 neutron capture process occurring in explosive-like stellar
 296 events. In the classical picture of the *r* process [41] a large
 297 burst of neutrons synthesizes the elements along a path
 298 determined by the $(n, \gamma) - (\gamma, n)$ equilibrium. After the
 299 exhaustion of neutrons these isotopes decay back to the
 300 valley of beta stability. In this simplified model the cap-
 301 ture cross section magnitude plays no role. However it is
 302 known [42–44] that for realistic irradiation scenarios the
 303 final elemental abundance is sensitive to the actual (n, γ)
 304 cross-sections. This is the case for the hot (classical) *r*
 305 process, due to the role of late captures during the decay
 306 back to stability. It is also the case for a cold *r*-process,
 307 where the formation path is determined by competition
 308 between neutron capture and beta decay.

309 Lacking experimental information, the cross section
 310 for these exotic nuclei is typically obtained from Hauser-
 311 Feshbach statistical model calculations [45]. This model
 312 is based on a few quantities describing average properties
 313 of the nucleus: the nuclear level density (NLD), the pho-
 314 ton strength function (PSF) and the neutron transmis-
 315 sion coefficient (NTC). The PSF determines Γ_γ , NTC de-
 316 termines Γ_n and NLD affects both (see Appendix). The
 317 parameters describing the dependence of these quantities
 318 on various magnitudes are adjusted to experiment close
 319 to β stability. It is thus crucial to find means to verify the
 320 predictions of the model far from stability. For example,
 321 the use of surrogate reactions with radioactive beams and
 322 inverse kinematics has been suggested as a tool to pro-
 323 vide experimental constraints on (n, γ) cross sections [46]
 324 for unstable nuclei, but its application is very challenging
 325 and, considering limitations on beam intensities, proba-
 326 bly limited to nuclei not far from stability at present. On
 327 the other hand the study of γ -ray emission from states
 328 above S_n observed in β decay can give quantitative infor-
 329 mation on $\Gamma_\gamma/\Gamma_{tot}$ for unstable nuclei. This information
 330 can be used to improve neutron capture cross-section es-
 331 timates for nuclei far away from β stability.

332 The emission of γ rays from neutron unbound states
 333 populated in β decay has been observed in very few cases
 334 studied with high-resolution germanium detectors. It
 335 was first detected in 1972 in the decay of ^{87}Br [47] which
 336 remains one of the best studied cases [48–50]. The other
 337 cases are: ^{137}I [51–53], ^{93}Rb [12, 54, 55], ^{85}As [52, 56],
 338 ^{141}Cs [57], ^{95}Rb [58], ^{94}Rb [55], ^{77}Cu [59], and ^{75}Cu [60].
 339 In the decay of ^{87}Br up to a dozen states emitting single
 340 γ -rays have been identified within 250 keV above S_n , with
 341 a total intensity of about 0.5% compared with a neutron
 342 emission intensity of 2.6%. The observation of relatively
 343 intense γ -rays in this measurement was explained as be-
 344 ing due to nuclear structure since some of the levels pop-

345 ulated could only decay through the hindered emission
 346 of a high orbital angular momentum neutron. On the
 347 other hand, it was pointed out [61] that a sizable γ -ray
 348 emission from neutron unbound states could be a mani-
 349 festation of Porter-Thomas (PT) statistical fluctuations
 350 in the strength of individual transitions. The extremely
 351 asymmetric shape of the PT distribution can lead to very
 352 large enhancement of the $\Gamma_\gamma/\Gamma_{tot}$ ratio with respect to
 353 the average. However a general characterization of the
 354 phenomenon is still lacking, in particular the relative im-
 355 portance of the different mechanisms governing the com-
 356 petition.

357 It is difficult to pursue these studies using HRGS be-
 358 cause of its reduced sensitivity. TAGS can offer the re-
 359 quired sensitivity at high excitation energy. However its
 360 application is challenging, since the expected γ branch-
 361 ing is very small. As a matter of fact previous attempts
 362 at the Leningrad Nuclear Physics Institute (LNPI) [55]
 363 did not lead to clear conclusions. As we have shown in
 364 Ref [9], and further discuss here, the TAGS technique can
 365 extract accurate information on the γ emission above S_n
 366 provided the possible sources of systematic error are un-
 367 der control.

368 The isotopes selected for this study are β -delayed neu-
 369 tron emitters with well known decay parameters (see Ta-
 370 ble I) that are located either close to the β -stability val-
 371 ley ($^{87,88}\text{Br}$) or relatively far away (^{94}Rb). In particu-
 372 lar ^{87}Br was included since it allows a comparison of
 373 our results with neutron capture and transmission ex-
 374 periments [50, 62] and with high resolution decay mea-
 375 surements [50]. An additional reason for their inclusion is
 376 that the spectrum of β -delayed neutrons is known [63, 64]
 377 for all of them and the neutron branching to the levels in
 378 the final nucleus has been studied [1–3]. This allows the
 379 reconstruction of the β intensity distribution followed by
 380 neutron emission and a more detailed comparison of γ to
 381 neutron branching ratios with calculations (See Section
 382 VII).

383 The case of ^{93}Rb was also measured [65] but will be
 384 presented separately.

385 II. MEASUREMENTS

386 The measurements were performed at the Cyclotron
 387 Laboratory of the University of Jyväskylä. The isotopes
 388 of interest are produced by proton-induced fission of Ura-
 389 nium in the ion-guide source of the IGISOL Mass Sep-
 390 arator [66]. The mass separated beam is guided to the
 391 JYFLTRAP Penning Trap [67], for suppression of con-
 392 tamination. The JYFLTRAP mass resolving power of
 393 few tens of thousands is sufficient to select the isotope of
 394 interest from the rest of isobars. The beam coming out
 395 of the trap is implanted at the centre of the spectrome-
 396 ter onto a movable tape, in between two rollers holding
 397 the tape in place. A cross-sectional view of the detection
 398 setup is shown in Fig. 1 and a detailed view of the beam-
 399 tube end-cap is shown in Fig 2. The tape is an ordinary

400 half-inch computer tape made of Mylar with a thickness
 401 of $30\ \mu\text{m}$ and a $10\ \mu\text{m}$ magnetic layer facing the beam.
 402 During the measurements the beam gate is open for a
 403 time period equivalent to three half-lives. This optimizes
 404 the counting of parent decays over descendant decays.
 405 After this period of time the tape transports the remain-
 406 ing activity away and a new measuring cycle starts. The
 407 tape moves inside an evacuated aluminium tube of 1 mm
 408 thickness and 47 mm diameter. Behind the tape implan-
 409 tation point is placed a 0.5 mm thick Si detector with
 410 a diameter of 25 mm, mounted on the aluminium end-
 411 cap. The β detection efficiency of the Si detector is about
 412 30%. The Valencia-Surrey Total Absorption Spectrome-
 413 ter “Rocinante” is a cylindrical 12-fold segmented BaF_2
 414 detector with a length and external diameter of 25 cm,
 415 and a longitudinal hole of 5 cm diameter. Each BaF_2
 416 crystal is optically isolated by means of a thin reflector
 417 wrapping, and viewed by a single 3” photo-multiplier
 418 tube (PMT). The crystals are mounted inside the alu-
 419 minium housing which has a 0.8 mm thick wall around
 420 the central hole. The total efficiency of “Rocinante” for
 421 detecting a single γ ray with the setup described here is
 422 larger than 80% in the energy range of interest. The spec-
 423 trometer is surrounded by 5 cm thick lead shielding to
 424 reduce the detection of the ambient background signals.

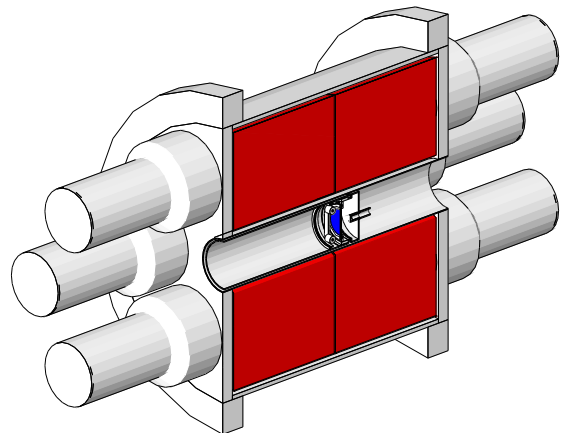


FIG. 1. (Color online) Cross-sectional view of the detector geometry as implemented in the Geant4 simulation code. BaF_2 crystals in red. Si detector in blue. The beam enters from the left and is deposited on the tape (not shown in the figure) in front of the Si detector.

425 The new spectrometer has a reduced neutron sensitiv-
 426 ity compared to existing instruments based on $\text{NaI}(\text{Tl})$
 427 crystals. This is a key feature in the present measure-
 428 ments as will be shown later. In addition, the segmen-
 429 tation of the detector allows one to obtain information
 430 on γ -ray cascade multiplicities which helps in the data
 431 analysis. The signal amplitudes from the 12 independent
 432 PMTs are digitized in a peak sensing analog-to-digital
 433 converter (ADC) and stored on disk for each event. The
 434 event trigger is provided whenever the hardware sum of
 435 the PMT signals fires a constant fraction discriminator

436 (CFD). The signal from the Si detector is processed in an
 437 analogous manner providing another trigger for read-out
 438 and storage of events. In the off-line analysis the PMT
 439 signals are gain matched and those surpassing a common
 440 threshold of 65 keV are added to obtain the total absorp-
 441 tion spectrum. The gain-matching procedure uses as a
 442 reference the position of the α -peaks visible in the en-
 443 ergy spectra coming from the Ra contamination always
 444 present in BaF₂ crystals. In order to eliminate this intrin-
 445 sic background as well as the ambient background we use
 446 in the present analysis β -gated total absorption spectra.
 447 The threshold in the Si β detector is set to 100 keV. Nev-
 448 ertheless other sources of background need to be taken
 449 into account.

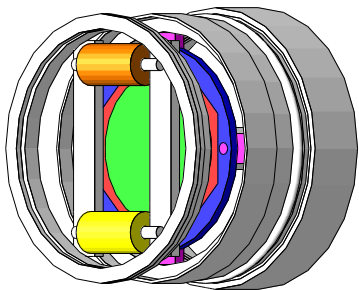


FIG. 2. (Color online) View of the beam-tube end-cap ge-
 ometry as implemented in the Geant4 simulation code. Vis-
 ible elements are: detector holder (blue), holder screws and
 mounts (pink), silicon detector (red) with active area (green),
 aluminium roller (yellow), plastic roller (orange), aluminium
 structural elements (white). For clarity the tape is not shown.

450 Firstly there is the decay descendant contamination,
 451 which was computed using Monte Carlo (MC) simula-
 452 tions performed with the Geant4 simulation toolkit [68].
 453 In the case of daughter decay contamination (⁸⁷Kr, ⁸⁸Kr,
 454 ⁹⁴Sr) we use an event generator based on β intensity dis-
 455 tributions and γ branching ratios obtained from the de-
 456 cay scheme in Ref. [1–3] which we assume is sufficiently
 457 well known. The normalization of the daughter contam-
 458 ination is estimated from the known half-lives and the
 459 measurement cycle time information and eventually ad-
 460 justed to provide the best fit to the recorded spectrum.
 461 The measurement of ⁸⁸Br was accidentally contaminated
 462 with ⁹⁴Y, the long-lived grand-daughter of ⁹⁴Rb that was
 463 measured immediately beforehand. It was treated in the
 464 same manner.

465 The contamination due to the β -delayed neutron
 466 branch is more challenging. The decay simulation must
 467 explicitly include the neutrons emitted. These neu-
 468 trons interact with detector materials producing γ -rays
 469 through inelastic and capture processes, which are read-
 470 ily detected in the spectrometer. The event generator
 471 should reproduce the known neutron energy distribution,
 472 taken from [64], the known γ -ray intensity in the final nu-
 473 cleus, taken from [1–3] and the correct decay sequence

474 $\beta \rightarrow$ neutron $\rightarrow \gamma$. Thus the event generator needs
 475 the β intensity distribution followed by neutron emission
 476 $I_{\beta n}(E_x)$. This can be obtained by deconvolution of the
 477 measured neutron energy spectrum $S(E_n)$, taking into
 478 account the relation

$$S(E_n) = \int_{S_n}^{Q_\beta} \left\langle \frac{\Gamma_n(E_x, E_n)}{\Gamma_n(E_x)} \right\rangle I_{\beta n}(E_x) dE_x \quad (5)$$

479 where $\langle \Gamma_n(E_x, E_n)/\Gamma_n(E_x) \rangle$ represents the neutron
 480 branching to levels in the final nucleus with excitation
 481 energy $E_x^f = E_x - S_n - E_n$ (see Appendix). The neu-
 482 tron branching ratio can be calculated using the Hauser-
 483 Feshbach model and this is done to obtain the $I_{\beta n}(E_x)$
 484 distribution used later in the present work. However the
 485 calculated $\langle \Gamma_n(E_x, E_n)/\Gamma_n(E_x) \rangle$ do not reproduce the
 486 observed γ -ray intensities in the final nucleus. Thus for
 487 the purpose of simulating the contamination due to β -
 488 delayed neutron decays we follow a different approach.
 489 We use the simplifying assumption that the neutron
 490 branching to each excited level in the final nucleus is
 491 independent of the excitation energy in the daughter nu-
 492 cleus. Then we can define partial decay intensities pro-
 493 portional to the neutron spectrum with energies larger
 494 than the excitation energy of the level f in the final nu-
 495 cleus, $I_{\beta n}^f(E_x) = I_n^f S(E_x - S_n - E_x^f)$. The proportional-
 496 ity constant I_n^f is just the measured neutron branching.
 497 The partial intensity to the ground state is obtained as
 498 the difference between the total neutron spectrum and
 499 the partial spectra. We found that the $I_{\beta n}(E_x)$ distribu-
 500 tion obtained in this manner is not very different from
 501 the one obtained by deconvolution.

502 A different issue related to the reproduction of the con-
 503 tamination coming from the β -delayed neutron branch is
 504 whether the interaction of neutrons with the detector can
 505 be simulated accurately. We have shown recently [69]
 506 this to be the case for a LaBr₃:Ce detector, provided
 507 that Geant4 is updated with the newest neutron data
 508 libraries and the original capture cascade generator is
 509 substituted by an improved one based on the nuclear sta-
 510 tistical model. We have followed the same approach for
 511 our BaF₂ detector. The normalization factor of the β -
 512 delayed neutron decay contamination is fixed by the P_n
 513 value.

514 An important source of spectrum distortion is the
 515 summing-pileup of events. If more than one event ar-
 516 rives within the same ADC event gate, a signal with
 517 the wrong energy will be stored in the spectrum. Apart
 518 from the electronic pulse pile-up effect for a single crys-
 519 tal, which can be calculated using the methodology de-
 520 scribed in [70], one must consider the summing of signals
 521 from different crystals. A new Monte Carlo procedure
 522 to calculate their combined contribution has been devel-
 523 oped. The procedure is based on the superposition of two
 524 recorded events, selected randomly. The time of arrival
 525 of the second event is sampled randomly within the ADC
 526 gate length. The normalization of the resulting summing-
 527 pileup spectrum is fixed by the true rate and the ADC

528 gate length [70]. To calculate the rate a dead time cor-
 529 rection is necessary and this is obtained by counting the
 530 signals from a fixed frequency pulse generator feeding the
 531 preamplifier. The use of real events to calculate the spec-
 532 trum distortion is valid if the actual summing-pileup rate
 533 is small enough. For this reason we kept the overall rate
 534 during the measurements below 7 kcps. The method is
 535 validated with measurements of laboratory sources.

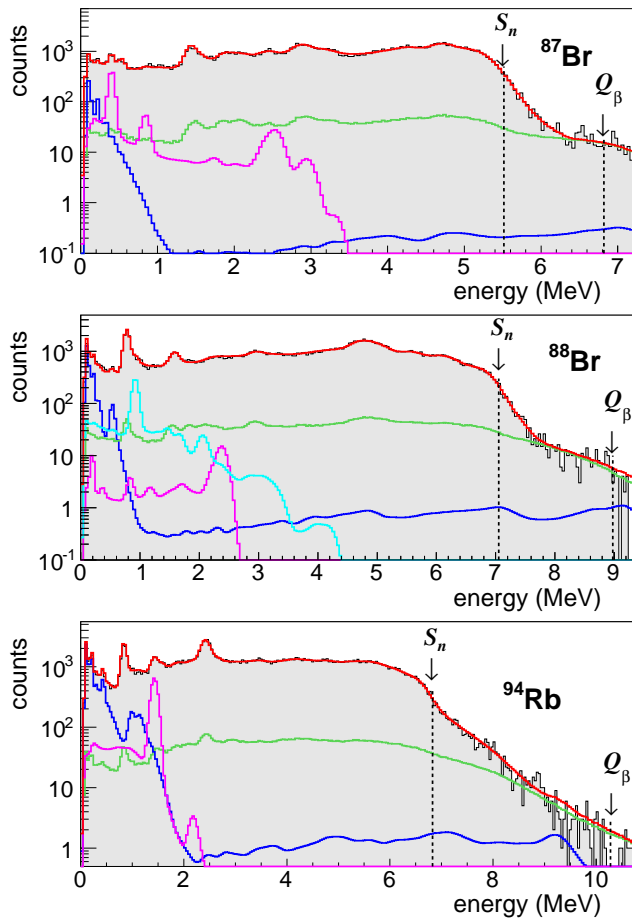


FIG. 3. (Color online) Relevant histograms for the analysis: parent decay (gray filled), daughter decay (pink), delayed neutron decay (dark blue), accidental contamination (light blue), summing-pileup contribution (green), reconstructed spectrum (red). See text for details. The neutron separation energy S_n and decay energy window Q_β are also indicated.

536 Several sources, ^{22}Na , ^{24}Na , ^{60}Co and ^{137}Cs , were
 537 used to determine both the energy calibration and the
 538 resolution versus energy dependency of the spectrom-
 539 eter. The latter is needed to widen the MC simulated
 540 response and is parametrized in the form of a Gaussian
 541 with $\sigma_E = \sqrt{aE + bE^2}$. The highest calibration point
 542 is at 4.123 MeV. At this energy the energy resolution
 543 (FWHM) is 265 keV which becomes 455 keV at 10 MeV.
 544 The ungated spectra measured with the sources serve also
 545 to verify the accuracy of the Geant4 MC simulations of
 546 the spectrometer response to the decay. This requires a

547 detailed description in the simulation code of all materi-
 548 als in the measurement setup including detectors and
 549 the tape transport system. Figures 1 and 2 show details
 550 of the geometry implemented in Geant4.

551 The use of β -gated spectra in the analysis requires
 552 additional verifications of the simulation. Due to the
 553 existence of an electronic threshold in the Si detector
 554 (100 keV) and the continuum nature of the β spectrum
 555 the efficiency for β -detection has a strong dependency
 556 with endpoint energy up to about 2 MeV. It should
 557 be noted that this affects the spectral region above S_n
 558 in which we are particularly interested. To investigate
 559 whether the MC simulation can reproduce this energy
 560 dependency accurately we used the information from a
 561 separate experiment [71] measuring P_n values with the
 562 neutron counter BELEN and the same β detector and
 563 implantation setup. Several β -delayed neutron emitters
 564 with known neutron energy spectra were measured, in-
 565 cluding ^{88}Br , $^{94,95}\text{Rb}$ and ^{137}I . They have different neu-
 566 tron emission windows $Q_\beta - S_n$, therefore the neutron-
 567 gated β efficiency samples different portions of the low
 568 energy part of the efficiency curve. Indeed the measured
 569 average β detection efficiency for each isotope changes by
 570 as much as 25%. Using the above mentioned β -delayed
 571 neutron decay generator in Geant4 we are able to repro-
 572 duce the isotope dependent efficiency to within better
 573 than 4%, determining the level of accuracy of the simu-
 574 lation.

575 Figure 3 shows the β -gated TAGS spectrum measured
 576 for all three isotopes. Also shown is the contribution to
 577 the measured spectra of the daughter decay, the neutron
 578 decay branch, and the summing-pileup effect. In the case
 579 of ^{88}Br it also includes the contribution of the accidental
 580 contamination with ^{94}Y decay. Note that there are net
 581 counts above the background beyond the neutron separ-
 582 ation energy. The fraction of counts that are to be
 583 attributed to states above S_n populated in the decay de-
 584 exciting by γ -ray emission is obtained after deconvolu-
 585 tion with the spectrometer response. In this region the ma-
 586 jor background contribution comes from summing-pileup
 587 which is well reproduced by the calculation as can be ob-
 588 served. The contribution of neutron capture γ -rays in
 589 the detector materials is much smaller, thanks to the low
 590 neutron sensitivity of BaF_2 , as can be seen. The contri-
 591 bution of γ -rays coming from neutron inelastic scattering
 592 is important at energies below 1 MeV.

593 III. ANALYSIS

594 The analysis of the β -gated spectra follows the method
 595 developed by the Valencia group [72, 73]. The deconvo-
 596 lution of spectra with the spectrometer response to the
 597 decay is performed using the Expectation-Maximization
 598 (EM) algorithm described there. The spectrometer re-
 599 sponse is constructed in two steps. First the response
 600 to electromagnetic cascades is calculated from a set of
 601 branching ratios and the MC calculated response to in-

dividual γ -rays. In the simulation we use a single crystal low energy threshold of 65 keV from experiment. When necessary, the electron conversion process is taken into account while building the response [74]. Branching ratios are taken from [1–3] for the low energy part of the level scheme. In the present case this involves 4 levels up to 1.6 MeV for ^{87}Kr , 8 levels up to 2.5 MeV for ^{88}Kr and 11 levels up to 2.8 MeV for ^{94}Sr . The excitation energy range above the last discrete level is treated as a continuum and is divided into 40 keV bins. Average branching ratios for each bin are calculated from the NLD and PSF as prescribed by the nuclear statistical model (see Appendix). We use the NLD calculated using a Hartree-Fock-Bogoliubov (HFB) plus combinatorial approach adjusted to experimental information [16, 75], which includes parity dependence. The PSF is obtained from Generalized Lorentzian (E1 transitions) or Lorentzian (M1 and E2 transitions) parametrization using the parameters recommended in the RIPL-3 reference input parameter library [16]. In the second step of the response construction, the previously obtained electromagnetic response for each level or energy bin is convoluted with the simulated response to a β continuum of allowed shape. The β response is obtained under the condition that the energy deposited in the Si detector is above the 100 keV threshold.

The spins and parities of some of the discrete states in the daughter nucleus are ambiguous but they are needed in order to calculate the branching ratio from states in the continuum. In the analysis different spin-parity values are tested and those giving the best fit to the spectrum are taken. The spin and parity of the parent nucleus ground state is also uncertain, however it determines the spin and parity of the states populated in the continuum needed to construct the branching ratio matrix. We assume that the Gamow-Teller selection rule applies for decays into the continuum, i.e., the parity does not change and the spin change fulfill $|\Delta J| \leq 1$. In the calculation of the branching ratios we further assume that different spins J are populated according to the spin statistical weight $2J + 1$. Our choices of spin and parity for the ground state are $3/2^-$ for ^{87}Br , 1^- for ^{88}Br and 3^- for ^{94}Rb , based again on the quality of reproduction of the measured spectra. The spin-parity of ^{87}Br is given as $3/2^-$ in Ref. [1], however Ref. [76] proposes $5/2^-$. We do not find significant differences in the analysis assuming these two values and we choose the former. The spin-parity of ^{88}Br is uncertain and is given as (2^-) in Ref. [2]. However Ref. [77] suggests 1^- . In our analysis we use the latter value since it clearly provides a much better reproduction of the measured TAGS spectrum. In the case of ^{94}Rb $3(-)$ is proposed [3] and is adopted, since other alternatives did not lead to a better reproduction of the spectrum.

In the analysis we permit decays to all discrete states, many of which are of the forbidden type. Forbidden transitions to the ground state or low lying excited states are known to occur in this region of the nuclear chart.

Indeed sizable decay intensity for some forbidden transitions is obtained in our analysis. In the case of ^{87}Br we find a ground state intensity $I_{\beta}^{gs} = 10.1\%$ quite close to 12%, the quoted value in Ref. [1]. However in contrast to [1], the first four excited states included in the discrete part receive negligible intensity. The summed decay intensity to the discrete part becomes 51% of that in Ref. [1]. In Ref. [2] an upper limit of 11% is given for the ^{88}Br ground state decay intensity, and a sizable intensity is quoted for some of the eight excited states included in the analysis. We obtain 4.7% and 5.6% for the β intensity to the ground state and first excited state respectively, and small or negligible intensity for the remaining states. Overall the intensity to this part of the level scheme is reduced by 64%. No intensity is assigned in [3] to ^{94}Rb decaying to the ground state (third forbidden) and first excited state (first forbidden). In our analysis we forbid the decay to those states after verifying that the decay intensity obtained when left free is only 0.5% and 0.02% respectively. A large decay intensity of 23.7% is observed for the allowed transition to the state at $E_x = 2414$ keV, even larger than the value of 21.4% found in [3]. The intensity to the discrete level scheme included in our analysis (11 states) is 78% of that in ENSDF.

In the final analysis we applied a correction to branching ratios deduced from the statistical model. The aim is to obtain a spectrometer response that is as realistic as possible. We scale the calculated branching ratios going from the unknown part of the level scheme to discrete levels in the known part of the level scheme, in order to reproduce the observed γ -ray intensities as tabulated in Ref. [1–3]. Here we are making the assumption that the absolute γ intensity is correctly determined in HRGS measurements for the lowest excited levels. We found that this adjustment did not lead to significant changes in the quality of reproduction of the measured TAGS spectra and has a small impact on the results of the deconvolution.

Figure 4 shows the final β intensity distribution $I_{\beta\gamma}(E_x)$ resulting from the deconvolution of TAGS spectra for all three isotopes with the chosen branching ratio matrices. The intensity is normalized to $(100 - P_n)\%$. In each case the spectrum reconstructed with this intensity distribution gives a good reproduction of the measured spectrum as can be seen in Fig. 3. The full β intensity distribution including statistical uncertainties is given as Supplemental Material to this article [78]. The uncertainty due to the statistics in the data is computed according the prescription given in Ref. [73] and is very small.

We evaluate the impact of several sources of systematic uncertainty on the shape of the β intensity distribution. These include both uncertainties in the calculated decay response and uncertainties in the subtraction of background components. To study their effect we follow a similar procedure in all the cases. The chosen systematic parameter is varied and a new deconvolution is performed

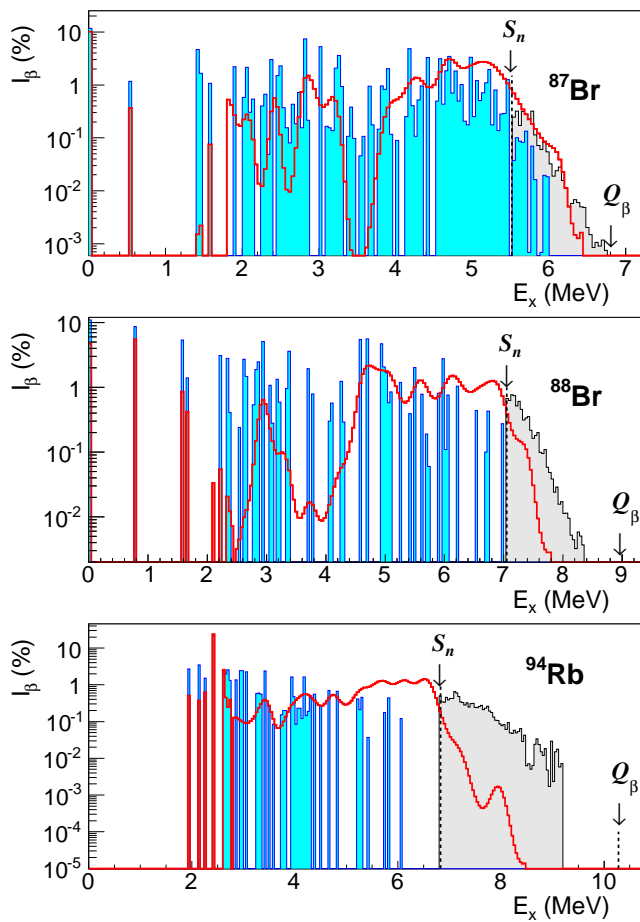


FIG. 4. (Color online) Beta intensity distributions: TAGS result (red line), high-resolution measurements (blue filled), from delayed neutron spectrum (gray filled). See text for details.

until we observe an appreciable deterioration in the reproduction of the measured spectrum. This is quantified by the increase of chi-square between the measured and reconstructed spectra. In this way we obtain the maximum acceptable deviation of the $I_{\beta\gamma}(E_x)$ from the adopted solution for each investigated systematic uncertainty. As a reference, the maximum chi-square increase found is always below 5%.

Uncertainties in the calculated decay response are of two types. Uncertainties in the branching ratio matrix, which were discussed above, and uncertainties in the MC simulation of the response to γ and β radiation. As already explained we take great care to describe accurately the geometry used in the Geant4 simulation, which is validated from the comparison with measurements with laboratory sources. However these sources emit β particles with rather low energies and they are not useful to verify the β response. The simulated β efficiency of the Si detector and in particular its variation with endpoint energy was studied in a separate measurement [71] as already discussed. The response of the spectrometer

to β particles depositing energy in the Si is not easy to verify. The response is a mixture of β penetration and secondary radiation produced in dead materials. The accurate simulation of the interaction of low energy electrons is a challenging task for any MC code. They rely on models to describe the slowing down of electrons and changes in their trajectory. Typically a number of tracking parameters are tuned to obtain reliable results. We use in the present simulations the *Livermore Electromagnetic Physics List* of Geant4 (version 9.2.p2) with original tracking parameters. This physics list has been developed for high accuracy tracking of low energy particles. We verified that limiting the tracking step length (parameter *StepMax*) to values much smaller than default values, increased computing time considerably but did not significantly affect the simulated response. Still the true response can differ from the simulation both in shape and magnitude and the differences can be endpoint energy dependent. To study the effect of a possible systematic error on the β response we take a crude approach, ignoring changes in shape and any dependence on endpoint energy. We scale arbitrarily the simulated spectrometer response while keeping the same β efficiency. In this way we find that solutions corresponding to changes of $\pm 10\%$ in the β response normalization represent the maximum deviation with respect to the adopted solution that can be accepted.

The individual γ response is well tested up to $E_\gamma = 2.754$ MeV, the maximum energy for the ^{24}Na source. To investigate the effect of a possible systematic error in the total γ efficiency ε_γ or in the peak-to-total ratio (P/T) we introduce a model that varies linearly one of the two parameters, ε_γ or P/T, above $E_\gamma = 3$ MeV. We found that variations of ε_γ amounting to $\pm 15\%$ at $E_\gamma = 10$ MeV or variations of P/T amounting to $\pm 30\%$ at the same energy are the maximum allowed by good reproduction of the spectrum. When considering these numbers one should bear in mind that the de-excitation of highly excited states populated in the decay of the three isotopes proceeds with an average γ multiplicity of 2 to 4 in such a way that the energy of most γ rays in the decay does not exceed 3 MeV.

Uncertainties in the normalization of background components also have an impact on the β intensity distribution. We consider the two main components, summing-pileup which affects the high energy part of the spectrum, and the β -delayed neutron decay branch, which affects the low energy part of the spectrum (see Fig. 3). The component due to summing-pileup is normalized using the same ADC gate length ($5 \mu\text{s}$) for all three isotopes. We estimate however that the reproduction of the end-part of the spectra allows for a variation of up to $\pm 15\%$ in the normalization factor. The normalization of the β -delayed neutron decay component is fixed by the P_n value. Likewise we find that the reproduction of the low energy part of the spectrum allows for a variation of up to $\pm 15\%$ in the normalization factor.

Finally we also check the impact on the result associ-

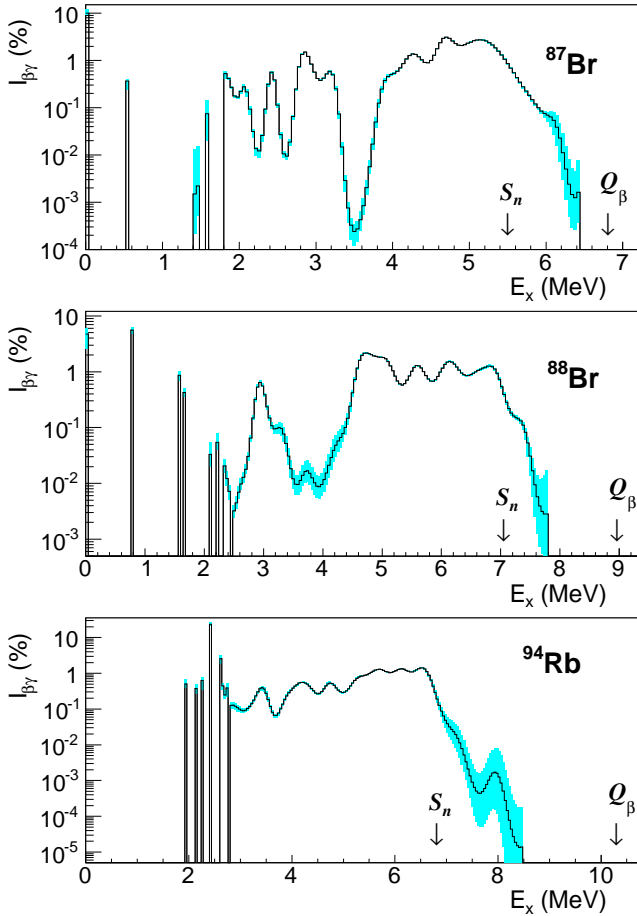


FIG. 5. (Color online) Beta intensity distributions from TAGS. The thin black line is the adopted solution, the light blue filled region indicates the spread of solutions due to the systematic effects investigated. See text for details.

ated with the use of a different deconvolution algorithm, by using the Maximum Entropy Method as described in Ref. [73]. This leads to changes in the $I_\beta(E_x)$ noticeable both at the high-energy end and at low E_x .

There is no straightforward way to quantify and combine the systematic uncertainties associated with the effects investigated. One of the reasons is that they are not independent since we are requiring reproduction of the data. It would have been a formidable task to explore in a correlated way the full parameter space. We use a different point of view here. The solutions we obtain through the systematic variation of each parameter represent maximum deviations from the adopted solution, thus altogether define an estimate of the space of solutions compatible with the data. This is represented in a graphical way in Fig. 5 showing the envelope of the different solutions described above corresponding to the maximum accepted deviation from the adopted solution. In total there are 14 solutions for ^{87}Br , 13 for ^{88}Br , and 15 for ^{94}Rb . As can be seen the different solutions differ little except for specific E_x regions, where the β inten-

sity is low, in particular at the high energy end of the distribution.

IV. AVERAGE BETA AND GAMMA DECAY ENERGIES AND DECAY HEAT

Figure 4 shows in addition to $I_{\beta\gamma}(E_x)$ obtained from our TAGS data the intensity obtained from HRGS measurements retrieved from the ENSDF data base [1–3]. The effect of *Pandemonium* is visible here. Our results show a redistribution of $I_{\beta\gamma}(E_x)$ towards high E_x , which is significant for ^{87}Br , and very large for ^{88}Br and ^{94}Rb . This is even clearer in the accumulated β intensity distribution as a function of excitation energy $I_{\beta\gamma}^\Sigma(E_x) = \int_0^{E_x} I_{\beta\gamma}(E)dE$, depicted in Fig. 6. The intensity is normalized to $100\% - P_n$ except in the case of the ^{94}Rb ENSDF intensity that only reaches 59.8% since the evaluators of Ref. [3] recognize the incompleteness of the decay scheme.

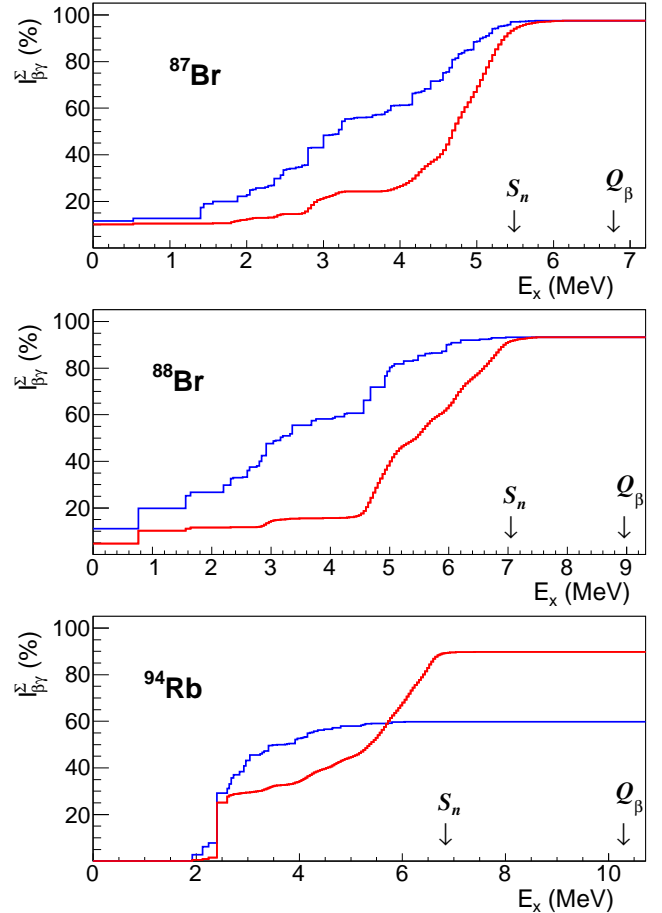


FIG. 6. (Color online) Accumulated β intensity distribution $I_{\beta\gamma}^\Sigma$: TAGS result (red line), high-resolution measurements (blue line).

Table II shows \bar{E}_γ and \bar{E}_β obtained from $I_{\beta\gamma}(E_x)$ using Eq. 1 and Eq. 2 respectively. The β continuum and its

837 average energy $\langle E_\beta(Q_\beta - E_x) \rangle$ for each E_x is calculated
 838 using subroutines extracted from the LOGFT program
 839 package maintained by NNDC (Brookhaven) [79]. In the
 840 calculations we assume an allowed β shape. As can be
 841 seen in Table II the redistribution of β intensity leads to
 842 large differences in the average emission energies when
 843 comparing HRGS data (ENSDF) and the present TAGS
 844 data. The difference has opposite directions for γ and β
 845 energies, as expected, except in the case of ^{94}Rb due to
 846 the use of a different normalization. For \bar{E}_γ the differ-
 847 ence is 0.9 MeV for ^{87}Br , 1.7 MeV for ^{88}Br , and 2.3 MeV
 848 for ^{94}Rb . The uncertainty quoted on the TAGS average
 849 energies in Table II is systematic since the contribution
 850 of statistical uncertainties in the case of $I_{\beta\gamma}(E_x)$ is negli-
 851 gible. The values of \bar{E}_γ and \bar{E}_β were computed for each
 852 intensity distribution that was used to define the space
 853 of accepted solutions in Fig. 5, and the maximum posi-
 854 tive and negative difference with respect to the adopted
 855 solution is the value quoted in the Table.

TABLE II. Average γ and β energies calculated using $I_{\beta\gamma}(E_x)$
 intensity distributions from ENSDF [1–3] and present TAGS
 data. The contribution of the β -delayed neutron branch is not
 included. Note that the ENSDF values for ^{94}Rb are obtained
 with a β intensity normalization of 59.8% (see text for details).

Isotope	\bar{E}_γ (keV)		\bar{E}_β (keV)	
	ENSDF	TAGS	ENSDF	TAGS
^{87}Br	3009	3938^{+40}_{-67}	1599	1159^{+32}_{-19}
^{88}Br	2892	4609^{+78}_{-67}	2491	1665^{+32}_{-38}
^{94}Rb	1729	4063^{+62}_{-66}	2019	2329^{+32}_{-30}

856 Table III shows the \bar{E}_β given in Ref. [38] obtained from
 857 the β spectrum measurements of Tengblad *et al.* [37].
 858 For comparison the average β energy obtained from the
 859 present TAGS data, given in Table II, is incremented with
 860 the average β energy corresponding to the β delayed neu-
 861 tron branch. The contribution of the βn branch is calcu-
 862 lated from the $I_{\beta n}(E_x)$ distribution obtained as explained
 863 in Section II. We find that the values of [38] agree with
 864 our result for ^{88}Br but differ by 240 keV for ^{87}Br and by
 865 380 keV for ^{94}Rb . This situation is comparable to that
 866 observed for Greenwood *et al.* [12] TAGS data. Figure 7
 867 presents in a graphical way the difference of average β
 868 energies $\Delta\bar{E}_\beta$ between the results of Tengblad *et al.* and
 869 the results of both Greenwood *et al.* and ourselves. In
 870 the figure the differences are represented as a function of
 871 Q_β to illustrate what seems a systematic trend. Although
 872 the scattering of values is relatively large, on average the
 873 differences are smaller below ~ 5 MeV. The isotopes from
 874 Ref. [12] shown in Fig. 7 are: ^{146}Ce , ^{145}Ce , ^{144}Ba , ^{141}Ba ,
 875 ^{143}La , ^{94}Sr , ^{93}Sr , ^{145}La , ^{143}Ba , ^{89}Rb , ^{141}Cs , ^{145}Ba , ^{91}Rb ,
 876 ^{95}Sr , ^{140}Cs , ^{90}Rb , ^{90m}Rb , and ^{93}Rb , in order of increas-
 877 ing Q_β .

878 More illustrative than the comparison of average val-
 879 ues is the comparison of β energy distributions $S_\beta(E_\beta)$ as

TABLE III. Comparison of average β energies obtained from
 direct β spectrum measurement (Tengblad *et al.* [38]) with
 those obtained combining $I_{\beta\gamma}(E_x)$ from present TAGS data
 and $I_{\beta n}(E_x)$ derived from neutron spectrum data. See text
 for details.

Isotope	\bar{E}_β (keV)	
	This work	Ref. [38]
^{87}Br	1170^{+32}_{-19}	1410 ± 10
^{88}Br	1706^{+32}_{-38}	1680 ± 10
^{94}Rb	2450^{+32}_{-30}	2830 ± 70

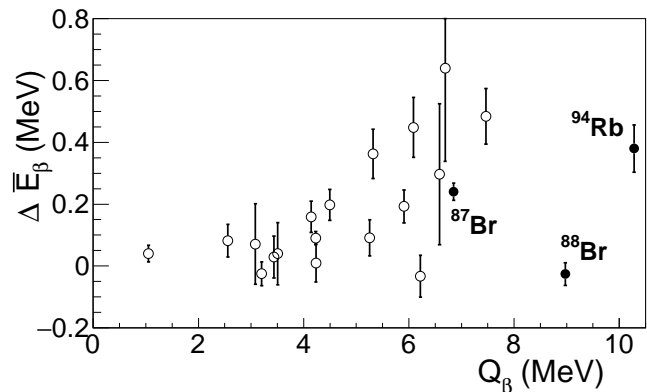


FIG. 7. Difference between average β energies obtained by
 direct β spectrum measurements (Tengblad *et al.* [38]) and
 from TAGS β intensity distributions. TAGS results are from
 [12] (open circles) and from the present work (filled circles).

880 is done in Fig. 8. Large differences in shape between the
 881 results of Tengblad *et al.* and the present TAGS results
 882 are clearly seen, even for ^{88}Br where the average values
 883 agree. The contribution of the β -delayed neutron branch,
 884 added to the TAGS result for the comparison, is shown.
 885 This contribution is calculated using the $I_{\beta n}(E_x)$ distri-
 886 bution obtained from the deconvolution of the known
 887 neutron spectrum (see Section II). For reference we also
 888 include in the figure the distribution calculated from the
 889 HRGS level scheme in ENSDF. The $S_\beta(E_\beta)$ distribution
 890 calculated from the TAGS data is shifted to lower ener-
 891 gies for the three isotopes, in comparison to the direct β
 892 spectrum measurement. We should point out that a simi-
 893 lar trend is found for the remaining isotopes included
 894 in the same experimental campaign, ^{86}Br and ^{91}Rb [80],
 895 and $^{92,93}\text{Rb}$ [36, 65], where we find deviations in $\Delta\bar{E}_\beta$
 896 in the range 200 to 400 keV. Moreover, our results for
 897 ^{91}Rb and ^{93}Rb agree rather well with those obtained by
 898 Greenwood *et al.* [12].

899 The assumption of an allowed shape used here to cal-
 900 culate $S_\beta(E_\beta)$ from $I_\beta(E_x)$ introduces some uncertainty
 901 in the comparison. However it is likely to be a good
 902 approximation. Thus to explain the difference between
 903 TAGS results and the direct β spectrum measurement

one is forced to consider systematic errors in the use of either one of the two techniques or both. As explained above we investigated carefully sources of systematic uncertainty which can lead to distortions of the β energy distribution and found that none of them can explain the observed differences (see Table III). Moreover as shown in Fig. 5 the measured TAGS spectrum imposes a strong constraint on the bulk of the β intensity distribution. It is difficult to imagine additional sources of systematic uncertainty which can have a significant impact on the shape of this distribution. To clarify the discrepancy new measurements of the spectrum of β particles emitted in the decay of a number of selected isotopes would be of great value.

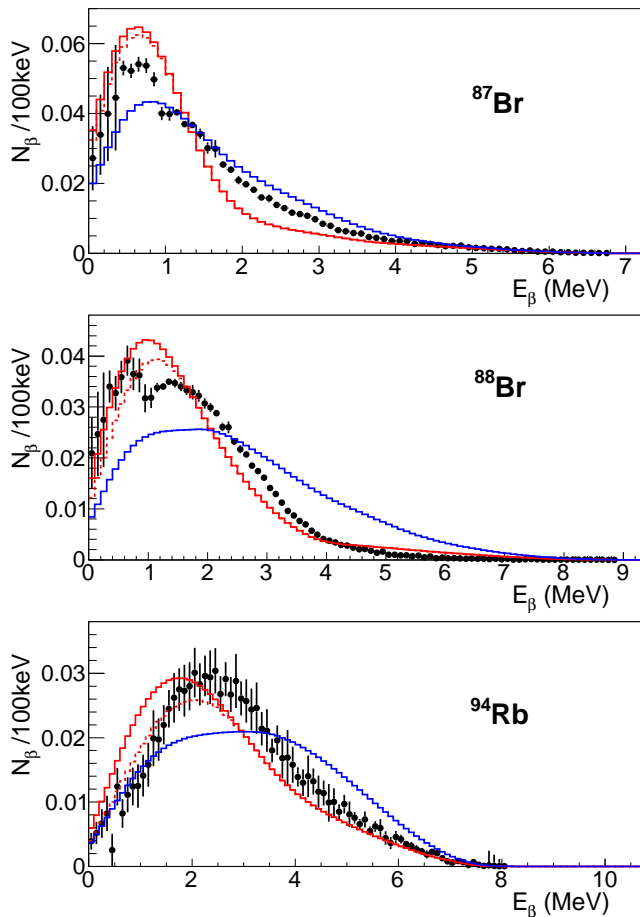


FIG. 8. (Color online) Comparison of β spectra S_β . Tengblad *et al.* [38]: black circles; present TAGS result: dashed red line; present TAGS plus β delayed neutron contribution: continuous red line; high-resolution measurements [1–3]: blue line.

To finalize this part of the discussion we should point out that \bar{E}_γ can be obtained from the β spectra measured in [37]. This can be achieved by deconvolution of the β spectra with appropriate β shapes $s_\beta(Q_\beta - E_x, E)$ to obtain the $I_\beta(E_x)$ (see Eq. 4). As a matter of fact this procedure is needed (and applied in [37]) to obtain

the antineutrino spectrum using Eq. 3. The average γ energies obtained in this way would show systematic differences with respect to TAGS results of opposite sign to those found for \bar{E}_β . Rather than using this approach the authors of [38] determine average γ energies \bar{E}_γ from an independent set of measurements using a NaI(Tl) detector to obtain the spectrum of γ -rays for the decay of each isotope. There are also large discrepancies between these results and those obtained from TAGS measurements. We postpone the discussion of these differences to a forthcoming publication [80].

The impact of the present TAGS results for \bar{E}_γ and \bar{E}_β on decay-heat summation calculations was evaluated. Figure 9 shows the ratio of calculations using TAGS data to calculations using HRGS data. The figure shows the evolution of the ratio as a function of cooling time following the prompt thermal fission of ^{235}U and ^{239}Pu . Both together account for most of the power released in most reactors. The calculation is similar to that described in Ref. [35]. It uses fission yields from JEFF-3.1 [81] and the ENDF/B-VII updated decay data sublibrary. The update introduces β -intensity distributions from previous TAGS measurements and, for a few isotopes, from β -spectrum measurements and from theoretical calculations. In the case of ^{87}Br , ^{88}Br and ^{94}Rb the data base adopts the ENSDF average γ and β energies from HRGS (Table II). As is customary the DH is evaluated separately for the electromagnetic energy (EEM), or photon component (γ rays, X rays, ...), and for the light particle energy (ELP), or electron component (β particles, conversion electrons, Auger electrons, ...). The ratio is computed for each individual isotope and for the three isotopes together. As expected the effect of the inclusion of TAGS data is largest for ^{94}Rb and smallest for ^{87}Br . The largest variation in the EEM component occurs at short cooling times between 1 and 10 s. Due to the particular normalization of the high-resolution ^{94}Rb β -intensity distribution mentioned above the effect is not observed in the ELP component (see also Table II). The effect is larger for ^{235}U fission, due to the larger fission yields for the three isotopes, reaching an increment of 3.3% for the combined contribution to the EEM component at $t = 3.5$ s. For ^{239}Pu the increment reaches 1.8%. Although the impact is somewhat small the present data contribute to reduce the discrepancy between DH integral measurements and summation calculations for ^{235}U in the range of 1 to 100 s (see for example Fig. 12 of Ref. [82]).

V. ANTINEUTRINO SPECTRA

The impact of our data on calculated antineutrino spectrum is shown in Fig. 10 and Fig. 11. The $\bar{\nu}_e$ summation calculation of Fig. 10 is analogous to the DH calculation of Fig. 9. It shows for ^{235}U and ^{239}Pu fission the ratio of calculated $\bar{\nu}_e$ spectrum when our TAGS data replaces HRGS data. The effect of each individual isotope

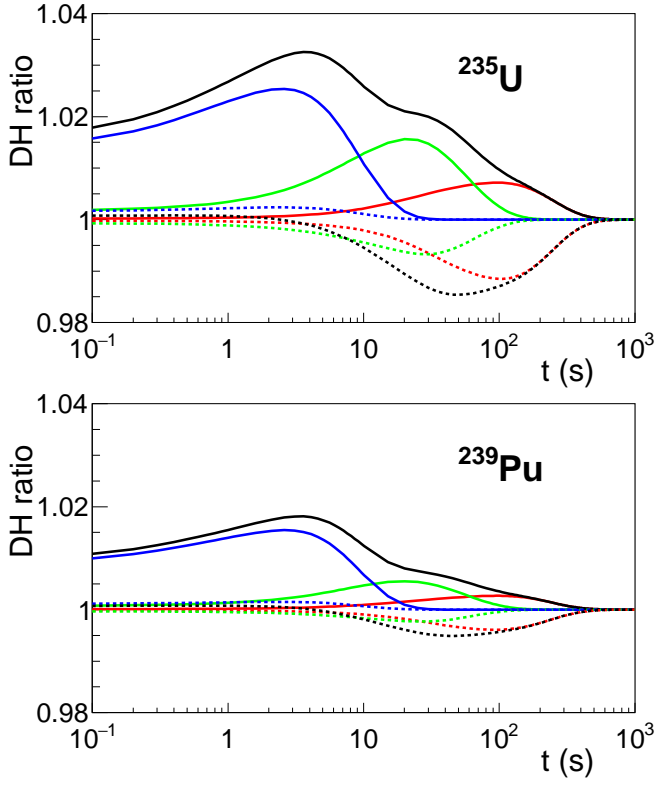


FIG. 9. (Color online) Ratio of decay heat as a function of cooling time calculated for ^{235}U and ^{239}Pu when our TAGS data replaces high-resolution data. Continuous line: photon component; dashed line: electron component. Red: ^{87}Br ; green: ^{88}Br ; blue: ^{94}Rb ; black: all three isotopes.

¹⁰⁰³ *Pandemonium* systematic error, even if they have mod-
¹⁰⁰⁴ erate fission yields.

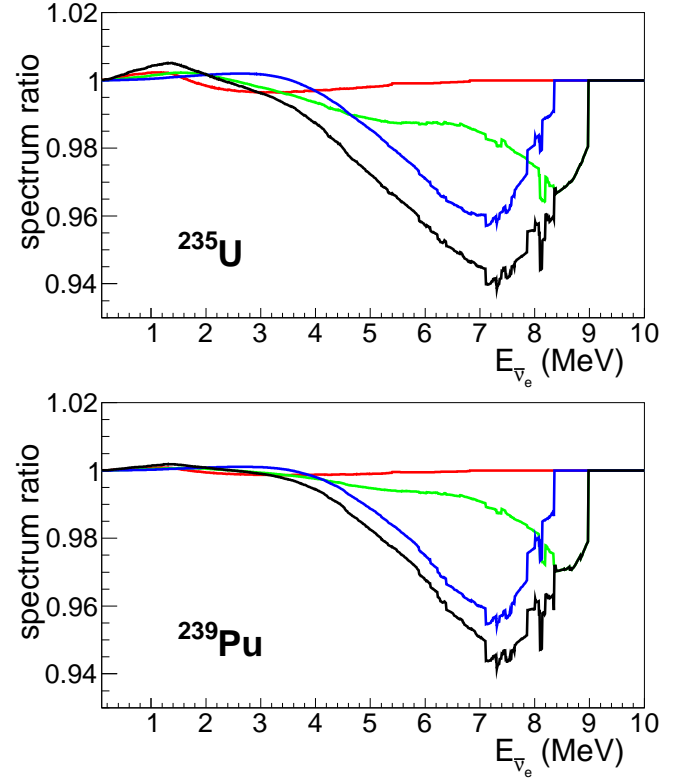


FIG. 10. (Color online) Ratio of antineutrino spectra as a function of energy calculated for ^{235}U and ^{239}Pu when our TAGS data replaces high-resolution data. Red: ^{87}Br ; green: ^{88}Br ; blue: ^{94}Rb ; black: all three isotopes.

and of the three together is shown. For both fissioning systems the impact of ^{87}Br is negligible, while the effect of ^{88}Br peaks around 8.5 MeV (3%) and that of ^{94}Rb peaks around 7 MeV (4%). The combined effect is a reduction of the calculated $\bar{\nu}_e$ spectrum which reaches a value of 6% around 7.2 MeV. Similar figures are obtained for ^{238}U and ^{241}Pu . It is remarkable that the effect of our TAGS data for ^{88}Br and ^{94}Rb is of equal importance to that of the combined effect of recently measured [83] TAGS data for ^{92}Rb , ^{96}Y and ^{142}Cs . Compare Fig. 10 in the present work with Fig. 6 of Ref. [83], which shows an effect of similar shape and magnitude. These three isotopes contribute most to the $\bar{\nu}_e$ spectrum around 7 MeV, with ^{92}Rb being the largest contributor [36]. Due to current uncertainties in the summation method it is not easy to draw conclusions on the impact of both experiments on the origin of the antineutrino spectrum shape distortion. Note that they lead to a *reduction* of the calculated spectrum which is maximum about 1 MeV above the center of the observed *excess*. Better quality data for a larger set of isotopes, including decay data and fission yields, is required. Our result shows the importance of performing TAGS measurements for fission products with very large Q_β -value, which are likely to be affected by large

Figure 11 shows a different set of $\bar{\nu}_e$ summation calculations. The calculation is analogous to that described in Ref. [29]. It uses a different selection of decay data from the calculation shown in Fig. 10. More specifically it uses antineutrino spectra derived from the β spectra of Tengblad *et al.* [37] for $^{87,88}\text{Br}$ and ^{94}Rb instead of $\bar{\nu}_e$ spectra derived from high-resolution data. Thus Fig. 11 shows the effect of replacing Tengblad *et al.* data with our TAGS data. As can be seen the replacement of ^{87}Br has little impact, while there is a cancellation below $E_{\bar{\nu}_e} = 8$ MeV between the ^{88}Br and ^{94}Rb deviations. However the difference between our TAGS data and the data of Tengblad *et al.* for ^{88}Br produces an increase in the calculated antineutrino spectra of about 7% between 8 and 9 MeV. Note that although ^{94}Rb has a Q_β of 10.28 MeV we do not observe appreciable β intensity below 2.41 MeV excitation energy, thus the maximum effective endpoint energy is below 8 MeV. The relatively large impact of ^{88}Br is due to the fact that only a few decay branches contribute to the spectrum here. Note that in this energy interval the uncertainty of the integral β -spectrum measurements [21, 22] is relatively large, thus summation calculations are particularly relevant. This

1028 points again to the need to perform TAGS measurements
1029 for fission products with very large Q_β .

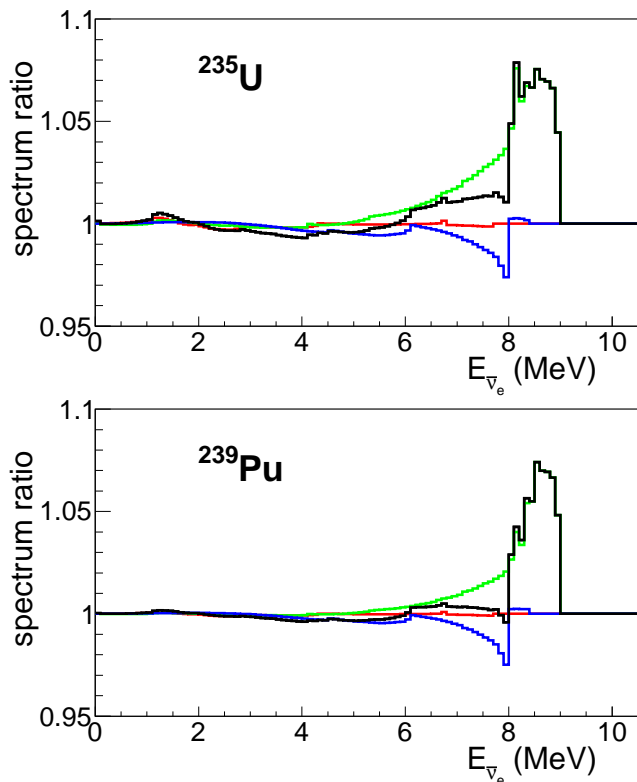


FIG. 11. (Color online) Ratio of antineutrino spectra as a function of energy calculated for ^{235}U and ^{239}Pu when our TAGS data replaces the data of Tengblad *et al.* Red: ^{87}Br ; green: ^{88}Br ; blue: ^{94}Rb ; black: all three isotopes.

1030 VI. GAMMA INTENSITY FROM NEUTRON 1031 UNBOUND STATES

1032 Figure 4 shows for all three isotopes a sizable TAGS
1033 intensity $I_{\beta\gamma}(E_x)$ above S_n . This intensity extends well
1034 beyond the first few hundred keV where the low neutron
1035 penetrability makes γ -ray emission competitive. For
1036 comparison the figure includes the β -intensity distribu-
1037 tion followed by neutron emission $I_{\beta n}(E_x)$ deduced from
1038 the neutron spectrum as explained above. The inte-
1039 grated decay intensity above S_n followed by γ -ray emis-
1040 sion $P_\gamma = \int_{S_n}^{Q_\beta} I_{\beta\gamma}(E_x) dE_x$ obtained from the TAGS
1041 measurement is compared to the integrated $I_{\beta n}(E_x)$ or
1042 P_n value in Table IV. Surprisingly large values of P_γ are
1043 obtained, which in the case of ^{87}Br is even larger than P_n .
1044 The γ branching represents 57% of the total for ^{87}Br , 20%
1045 for ^{87}Br and 4.5% for ^{94}Rb . In the case of ^{87}Br we find
1046 8 times more intensity than the high-resolution experi-
1047 ment [50], which can be explained by the *Pandemonium*
1048 effect. The quoted uncertainty on the TAGS integrated

1049 intensity P_γ is completely dominated by systematic un-
1050 certainties since the uncertainty due to data statistics is
1051 below 0.6% (relative value) in all cases.

TABLE IV. Integrated β -intensity P_γ from TAGS data above S_n compared to P_n values from [1–3].

Isotope	P_γ (%)	P_n (%)
^{87}Br	3.50^{+49}_{-40}	2.60(4)
^{88}Br	1.59^{+27}_{-22}	6.4(6)
^{94}Rb	0.53^{+33}_{-22}	10.18(24)

1052 We have evaluated several sources of systematic uncer-
1053 tainty. In the first place we consider uncertainties that
1054 affect the overall β intensity distributions, which were
1055 already detailed in Section III. To quantify the uncer-
1056 tainties in P_γ coming from the spread of possible solu-
1057 tions compatible with the data (see Fig 5) we follow the
1058 approach used in Section IV and take the maximum posi-
1059 tive and negative difference with respect to the adopted
1060 solution as a measure of this uncertainty.

1061 In addition to this we consider other sources of uncer-
1062 tainty which mostly affect the integral value.

1063 A possible source of uncertainty is related to the corre-
1064 lations introduced by the finite energy resolution in the
1065 deconvolution process. This can cause a relocation of
1066 counts in a region of rapidly changing intensity [73], such
1067 as the region around S_n . However we estimate from a
1068 model deconvolution that this effect is not relevant in the
1069 present case. Likewise the uncertainty on width calibra-
1070 tion also has an impact on the redistribution of counts
1071 around S_n . The highest width calibration point is at
1072 4.123 MeV. From the comparison of different fits, vary-
1073 ing the number and distribution of calibration points, we
1074 determine that the extrapolation of the calibration curve
1075 can vary by up to $\pm 15\%$ at 10 MeV. This introduces an
1076 uncertainty in P_γ of 2% for ^{87}Br and 6% for ^{88}Br and
1077 ^{94}Rb .

1078 The uncertainty in the energy calibration of TAGS
1079 spectra might have an impact on the result because of
1080 the dependence of the response on energy. However we
1081 verified that this effect is negligible. The main effect of
1082 the uncertainty on the energy calibration is on the inte-
1083 gration range. Since the intensity is rapidly changing in
1084 the region around S_n the effect can be large. The fact
1085 that the structure observed in the distribution of Fig. 12
1086 around 7–8 MeV for ^{94}Rb coincides with the levels pop-
1087 ulated in the final nucleus (see next Section) allows us
1088 to conclude that the energy calibration at S_n is correct
1089 to about one energy bin (40 keV). We evaluate the un-
1090 certainty in the integral, equivalent to changes of half
1091 a bin, to be 11% for the bromine isotopes and 15% for
1092 rubidium.

1093 The uncertainty values entered in Table IV correspond
1094 to the sum in quadrature of the three types of uncertainty

1095 mentioned above: uncertainties in the deconvolution, and
 1096 uncertainties in the resolution and energy calibration.

1097 VII. COMPARISON WITH 1098 HAUSER-FESHBACH CALCULATIONS

1099 We show in Fig. 12 the ratio $I_{\beta\gamma}(E_x)/(I_{\beta\gamma}(E_x) +$
 1100 $I_{\beta n}(E_x))$ as a function of excitation energy. The shaded
 1101 area represents the uncertainty in the ratio coming from
 1102 the spread of solutions $I_{\beta\gamma}(E_x)$ to the TAGS inverse
 1103 problem shown in Fig. 5. It should be noted that the
 1104 ratio is affected also by systematic uncertainties in the
 1105 $I_{\beta n}(E_x)$ distribution coming from the deconvolution of
 1106 neutron experimental spectra as well as by uncertainties
 1107 in the neutron spectra themselves, but they are not con-
 1108 sidered here.

1109 The experimental intensity ratio in Fig. 12 is identical
 1110 to the average ratio $\langle\Gamma_\gamma(E_x)/\Gamma_{tot}(E_x)\rangle$. The average is
 1111 taken over all levels in each bin populated in the decay.
 1112 Thus the experimental distribution can be directly com-
 1113 pared with the results of Hauser-Feshbach calculations
 1114 of this ratio. The NLD and PSF used in the calcula-
 1115 tions are the same as used to construct the spectrom-
 1116 eter response to the decay (see Section III). The new
 1117 ingredient needed is the NTC which is obtained from
 1118 the Optical Model (OM). It is calculated with Raynal's
 1119 ECIS06 OM code integrated in the TALYS-1.4 software
 1120 package [84]. OM parameters are taken from the so-called
 1121 local parametrization of Ref. [85]. Neutron transmission
 1122 is calculated for final levels known to be populated in the
 1123 decay: g.s. of ^{86}Kr , g.s and first excited state of ^{87}Kr ,
 1124 and g.s. plus 8 excited states of ^{93}Sr . With these ingre-
 1125 dients one obtains the average widths $\langle\Gamma_\gamma\rangle$ and $\langle\Gamma_n\rangle$ (see
 1126 Appendix).

1127 In the case of ^{87}Kr we can compare the calculated
 1128 average values with experimental data obtained from neu-
 1129 tron capture and transmission reactions [50, 62]. In par-
 1130 ticular for $1/2^-$ and $3/2^-$ resonances which are popu-
 1131 lated in the decay of a $3/2^-$ ^{87}Br ground state. Up
 1132 to fifty $1/2^-$ and sixty-six $3/2^-$ resonances were iden-
 1133 tified in an interval of 960 keV above S_n . The NLD of
 1134 Ref. [75] predicts 46 and 90 respectively, in fair agree-
 1135 ment with these values. The distribution of neutron widths for
 1136 $1/2^-$ resonances in the interval $E_n = 250 - 960$ keV is
 1137 compatible with a PT distribution with average width
 1138 $\langle\Gamma_n\rangle = 1.95$ keV. The same is true for $3/2^-$ resonances
 1139 with $\langle\Gamma_n\rangle = 2.79$ keV. In the same interval the Hauser-
 1140 Feshbach calculated widths vary between 0.3 keV and
 1141 0.7 keV for $1/2^-$ states and between 0.5 keV and 0.9 keV
 1142 for $3/2^-$ states. In both cases the calculation is about
 1143 4 times too low. The information on $\langle\Gamma_\gamma\rangle$ is less abun-
 1144 dant. The γ width has been determined for six $1/2^-$
 1145 and ten $3/2^-$ resonances, with values in the range 0.075-
 1146 0.48 eV, and is fixed to 0.255 eV, from systematics, for
 1147 the remaining resonances. The Hauser-Feshbach calcula-
 1148 tion gives values in the range 0.08-0.12 eV. On average
 1149 the calculation is about a factor three too low. Since

1150 the NLD reproduces the number of resonances, to reach
 1151 such values for the partial widths requires a renormal-
 1152 ization by a factor of 3-4 for the PSF and the NTC in
 1153 ^{87}Kr , which seems large. The reader should note that
 1154 variations of similar magnitude and direction for both
 1155 the PSF and NTC have little impact on the calculated
 1156 ratio $\langle\Gamma_\gamma/\Gamma_{tot}\rangle$. It should also be noted that this ratio is
 1157 insensitive to changes in NLD.

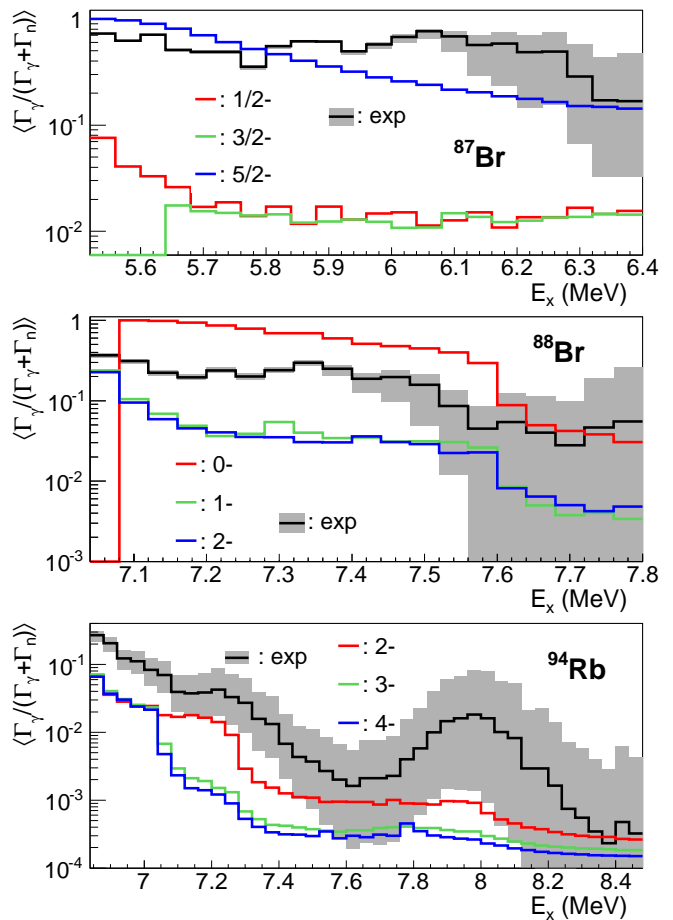


FIG. 12. (Color online) Average gamma to total width from experiment (black line) and calculated for the three spin-parity groups populated in allowed decay (red, green, blue). The gray-shaded area around the experiment indicates the sensitivity to systematic effects. See text for details.

1158 We show in Fig. 12 the ratio $\langle\Gamma_\gamma/\Gamma_{tot}\rangle$, calculated with
 1159 nuclear statistical parameters as described above, for the
 1160 three spin-parity groups populated under the Gamow-
 1161 Teller selection rule. Due to statistical fluctuations affect-
 1162 ing individual widths [61], this cannot be obtained
 1163 as $\langle\Gamma_\gamma\rangle/(\langle\Gamma_\gamma\rangle + \langle\Gamma_n\rangle)$. Rather than trying to obtain a
 1164 formula for the average correction factor to be applied
 1165 to this ratio, which is the common practice for cross sec-
 1166 tion calculations [84], we use the Monte Carlo method to
 1167 obtain directly the average of width ratios. The proce-
 1168 dure to obtain a statistical realization (or sample) from
 1169 the model is similar to that described in Ref. [72]. Level

energies for each spin-parity are generated according to a Wigner distribution from the NLD. For each state the corresponding Γ_γ and Γ_n to individual final states are sampled from PT distributions with the calculated average values (see Appendix). The total γ and neutron widths are obtained by summation over all possible final states and the ratio is computed. The ratio is averaged for all levels lying within each energy bin (40 keV). In order to eliminate fluctuations in the calculated averages, the procedure is repeated between 5 and 1000 times depending on level density. Very large average enhancement factors are obtained, reaching two orders-of-magnitude, when the neutron emission is dominated by the transition to a single final state.

In the case of the decay of the $3/2^-$ ground state in ^{87}Br one can see in Fig. 12 that the strong γ -ray emission above S_n can be explained as a consequence of the large hindrance of $l = 3$ neutron emission from $5/2^-$ states in ^{87}Kr to the 0^+ g.s. of ^{86}Kr . This is the explanation already proposed in [50]. The situation is even more favorable to this explanation if the spin-parity of ^{87}Br were $5/2^-$ as suggested in [76]. In this case the neutron emission is hindered for both $5/2^-$ and $7/2^-$ states populated in the allowed decay. In the case of ^{88}Br 1^- decay a similar situation occurs for 0^- states in ^{88}Kr below the first excited state in ^{87}Kr at 532 keV, which requires $l = 3$ neutron emission to populate the $5/2^+$ g.s. in ^{87}Kr . It should be noted that if the spin-parity of ^{88}Br were 2^- as suggested in [2] the three allowed spin-parity groups (1^- , 2^- , 3^-) will have similar gamma-to-total ratios, a factor of 3 to 5 too low compared to experiment, which reinforces our choice of 1^- for the ^{88}Br g.s. A more quantitative comparison of the experimental and calculated ratios requires a knowledge of the distribution of β intensity between the three spin groups. This can be obtained from β strength theoretical calculations, such as those in [86] for example. It is clear however that for both bromine isotopes the large γ branching above S_n can be explained as a nuclear structure effect: the absence of states in the final nucleus which can be populated through the emission of neutrons of low orbital angular momentum.

The case of ^{94}Rb 3^- decay is the most interesting. The final nucleus ^{93}Sr is five neutrons away from β stability. Although the γ intensity is strongly reduced, only 5 % of the neutron intensity, is detectable up to more than 1 MeV above S_n . The structure observed in the distribution of the average ratio $\langle \Gamma_\gamma / \Gamma_{tot} \rangle$, can be associated with the opening of βn channels to different excited states in ^{93}Sr . As can be seen the structure is reproduced by the calculation, which confirms the energy calibration at high excitation energies. In any case the calculated average gamma-to-total ratio is well below the experimental value. In order to bring the calculation in line with the experimental value one would need to enhance the γ width, or suppress the neutron width, or any suitable combination of the two, by a very large factor of about one order-of-magnitude. A large enhancement of the γ

width, and thus of the calculated (n, γ) cross sections, would have an impact on r process abundance calculations [42–44]. It would be necessary to confirm the large enhancement of the $\langle \Gamma_\gamma / \Gamma_{tot} \rangle$ ratio observed in ^{94}Rb with similar studies on other neutron-rich nuclei in this mass region as well as in other mass regions. It will also be important to quantify the contribution of a possible suppression of the neutron width to the observed ratio.

VIII. SUMMARY AND CONCLUSION

We apply the TAGS technique to study the decay of three β -delayed neutron emitters. For this we use a new segmented BaF_2 spectrometer with reduced neutron sensitivity, which proved to be well suited to this purpose. The three isotopes, ^{87}Br , ^{88}Br and ^{94}Rb , are fission products with impact in reactor decay heat and antineutrino spectrum summation calculations. We obtain β intensity distributions which are free from the *Pandemonium* systematic error, affecting the data available in the ENSDF data base for the three isotopes. The average γ -ray energies that we obtain are 31%, 59% and 235% larger than those calculated with this data base for ^{87}Br , ^{88}Br and ^{94}Rb respectively, while the average β energies are 28%, 33% and 13% smaller.

We compare the energy distribution of β particles emitted in the decay derived from our β intensity distributions with the direct β spectrum measurement performed by Tengblad *et al.*, and find significant discrepancies. Our distributions are shifted to somewhat lower energies. This is reflected in the average β energies, which we find to be 17% and 13% smaller for ^{87}Br and ^{94}Rb respectively. Similar systematic differences are found when the TAGS data of Greenwood *et al.* for 18 isotopes is compared with the data of Tengblad *et al.* We performed a thorough investigation of possible systematic errors in the TAGS technique and find that none of them can explain the observed differences. It will be important to perform new direct measurements of the β spectrum for a few selected isotopes in order to investigate this issue further.

We estimate the effect of the present data on DH summation calculations. We find a relatively modest impact when the high resolution decay data are replaced by our TAGS data. The impact in the photon component is largest at short cooling times. For ^{235}U thermal fission it reaches an increment of 3.3% around 3.5 s after fission termination. This is mainly due to the decay of ^{94}Rb . The influence of ^{88}Br is smaller and peaks at around 25 s. In spite of being small it contributes to reduce the discrepancy between DH integral measurements of the EEM component and summation calculations for ^{235}U in the range of 1 to 100 s. Many FP contribute in this time range, thus additional TAGS measurements of short lived FP are required to remove the discrepancy. In the case of ^{239}Pu the maximum increment is about 1.8%.

We also evaluate the impact of the new TAGS data on

antineutrino spectrum summation calculations. When our data replace the data from high-resolution measurements we observe a reduction of the calculated $\bar{\nu}_e$ spectrum which reaches a maximum value of 6% at 7 MeV for the thermal fission of ^{235}U . A similar value is obtained for ^{239}Pu . The reduction is mainly due to the decay of ^{94}Rb . The effect of ^{88}Br , somewhat smaller, peaks at 8.5 MeV. It is remarkable that we find an impact similar to that observed recently for ^{92}Rb , ^{96}Y and ^{142}Cs together, which make the largest contribution to the antineutrino spectrum at these energies. The reason is that the large value of the *Pandemonium* systematic error prevails over the relatively small fission yield for the isotopes studied in the present work. We also verified the effect of replacing our TAGS data with Tengblad *et al.* β -spectrum data. We found a relatively small impact below $E_{\bar{\nu}_e} = 8$ MeV in part due to a compensation effect of the deviations for ^{94}Rb and ^{88}Br . However between 8 and 9 MeV the use of TAGS data for ^{88}Br leads to an increase of about 7% in the calculated antineutrino spectrum. This relatively large impact is due to the small number of decay branches in this energy range. All this underlines the need for TAGS measurements for fission products with a very large Q_β decay energy window.

We confirm the suitability of the TAGS technique for obtaining accurate information on γ -ray emission from neutron-unbound states. In order to assess the reliability of the result we examined the systematic errors carefully since they dominate the total uncertainty budget. Surprisingly large γ -ray branchings of 57% and 20% were observed for ^{87}Br and ^{88}Br respectively. In the case of ^{94}Rb the measured branching of 4.5% is smaller but still significant. For ^{87}Br we observe 8 times more intensity than previously detected with high resolution γ -ray spectroscopy, which confirms the need to use the TAGS technique for such studies.

Combining the information obtained from TAGS measurements about the γ intensity from states above S_n with the β -delayed neutron intensity we can determine the branching ratio $\langle \Gamma_\gamma / (\Gamma_\gamma + \Gamma_n) \rangle$ as a function of E_x . The information thus acquired, can be used to constrain the neutron capture cross-section for unstable neutron-rich nuclei. This opens a new field for applications of β -decay TAGS studies. It also provides additional arguments for the need for accurate measurements of β -delayed neutron emission in exotic nuclei. The measurements should cover neutron spectra and yields as well as neutron- γ coincidences.

From the comparison of our experimental results with Hauser-Feshbach calculations we conclude that the large γ branching observed in ^{87}Br and ^{88}Br is a consequence of the nuclear structure. Some of the resonances populated in the decay can only disintegrate via the emission of a kinematically hindered neutron to the levels available in the final nucleus. A similar situation can occur for other β -delayed neutron emitters, when the number of levels in the final nucleus within the emission window $Q_\beta - S_n$ is small. It should be noted that such strong γ

to neutron competition introduces a large correction to the estimation of β -delayed neutron emission probabilities from β -strength calculations and should be taken into account when comparing experiment with calculation.

The case of ^{94}Rb , is more representative of the situation expected for nuclei far from stability, where many levels are available thus the decay by low l neutron emission is always possible. For ^{94}Rb we find that the γ -ray emission from neutron-unbound states is largely suppressed, but still much larger (an order-of-magnitude) than the result of Hauser-Feshbach calculations using standard parameters for level density, photon strength and neutron transmission. If such enhancement with respect to the Hauser-Feshbach model is due mainly to an increment in the radiative width, then a similar increase is obtained for the neutron capture cross-section. This can have a significant impact on calculated elemental abundances in the astrophysical r process. It is necessary to confirm and generalize the result obtained for the neutron-rich nucleus ^{94}Rb extending this type of study to other β -delayed neutron emitters in the same and different mass regions, in particular farther away from the valley of β -stability. Such measurements using the TAGS technique are already underway and additional studies are planned.

ACKNOWLEDGMENTS

This work was supported by Spanish Ministerio de Economía y Competitividad under grants FPA2008-06419, FPA2010-17142, FPA2011-24553, FPA2014-52823-C2-1-P, CPAN CSD-2007-00042 (Ingenio2010) and the program Severo Ochoa (SEV-2014-0398). WG would like to thank the University of Valencia for support. This work was supported by the Academy of Finland under the Finnish Centre of Excellence Programme 2012-2017 (Project No. 213503, Nuclear and Accelerator-Based Physics Research at JYFL). Work supported by EP-SRC(UK) and STFC(UK). Work partially supported by the European Commission under the FP7/EURATOM contract 605203. FGK acknowledges support from the U.S. Department of Energy, under contract number DE-AC02-06CH11357. We thank David Lhuillier for making available in digital form data tabulated in Ref. [38]. The authors would like to thank the late Olivier Bersillon for drawing our attention to the inconsistencies between average decay energies obtained from Ref. [38] and from Ref. [12].

APPENDIX

The average γ width for initial levels (resonances) of spin-parity J_i^π at excitation energy E_x can be obtained by summation over all final states of spin-parity J_f^π and excitation energy $E_x - E_\gamma$:

1404 by summation over all final states of spin-parity J_f^π and
1405 excitation energy $E_x - S_n - E_n$ in the final nucleus:

$$\begin{aligned} \langle \Gamma_\gamma(J_i^\pi, E_x) \rangle &= \sum_f \langle \Gamma_\gamma(J_i^\pi, E_x, E_\gamma) \rangle \\ &= \frac{1}{\rho(J_i^\pi, E_x)} \sum_f \sum_{XL} E_\gamma^{2L+1} f_{XL}(E_\gamma) \end{aligned} \quad (6)$$

$$\begin{aligned} \langle \Gamma_n(J_i^\pi, E_x) \rangle &= \sum_f \langle \Gamma_n(J_i^\pi, E_x, E_n) \rangle \\ &= \frac{1}{2\pi\rho(J_i^\pi, E_x)} \sum_f \sum_{ls} T^{ls}(E_n) \end{aligned} \quad (8)$$

1392 where $\rho(J_i^\pi, E_x)$ represents the density of initial levels
1393 and $f_{XL}(E_\gamma)$ is the photon strength for transition energy
1394 E_γ . The appropriate electric or magnetic character X
1395 and multipolarity L of the transition is selected by spin
1396 and parity conservation. We have used the common prac-
1397 tice of restricting the transition types to E1, M1 and E2
1398 with no mixing, which leads to a single XL choice for
1399 each final state.

1400 For transitions into a bin of width ΔE in the contin-
1401 uum part of the level scheme the density weighted aver-
1402 age over final levels should be used:

$$\begin{aligned} \langle \Gamma_\gamma(J_i^\pi, E_x) \rangle &= \frac{1}{\rho(J_i^\pi, E_x)} \sum_f \sum_{XL} \int_E^{E+\Delta E} E_\gamma^{2L+1} \\ &\quad \times f_{XL}(E_\gamma) \rho(J_f^\pi, E_x - E_\gamma) dE_\gamma \end{aligned} \quad (7)$$

1406 where $T^{ls}(E_n)$ is the neutron transmission coefficient,
1407 a function of neutron energy E_n . The orbital angular
1408 momentum l and channel spin s are selected by spin and
1409 parity conservation for each final level.

1410 The average over initial spin-parities J_i^π at each E_x
1411 is obtained using the corresponding weights $w(J_i^\pi, E_x)$,
1412 properly normalized $\sum_i w(J_i^\pi, E_x) = 1$, from

$$\langle \Gamma_\gamma(E_x) \rangle = \sum_i w(J_i^\pi, E_x) \langle \Gamma_\gamma(J_i^\pi, E_x) \rangle \quad (9)$$

$$\langle \Gamma_n(E_x) \rangle = \sum_i w(J_i^\pi, E_x) \langle \Gamma_n(J_i^\pi, E_x) \rangle \quad (10)$$

1403 Likewise the average neutron width can be obtained

-
- 1413 [1] R. G. Helmer, Nucl. Data Sheets **95**, 543 (2002).
1414 [2] E.A. McCutchan and A.A. Sonzogni, Nucl. Data Sheets
1415 **115**, 135 (2014).
1416 [3] D. Abriola and A.A. Sonzogni, Nucl. Data Sheets **107**,
1417 2423 (2006).
1418 [4] J. Hardy *et al.*, Phys. Lett. B **71**, 307 (1977).
1419 [5] C. L. Duke *et al.*, Nucl. Phys. A **151**, 609 (1970).
1420 [6] A. Algora *et al.*, Nucl. Phys. A **654**, 727c (1999).
1421 [7] A. Algora *et al.*, Phys. Rev. C **68**, 034301 (2003).
1422 [8] Z. Hu *et al.*, Phys. Rev. C **60**, 024315 (1999).
1423 [9] J. L. Tain *et al.*, Phys. Rev. Lett. **115**, 062502 (2015).
1424 [10] K. Okumura *et al.*, *Proceedings of the 2012 Sympo-*
1425 *sium on Nuclear Data, Kyoto*, JAEA-Conf 2013-002,
1426 INDC(JPN)-198, p. 15, 2013.
1427 [11] T. Yoshida and R. Nakasima, J. Nucl. Sci. Technol., **18**,
1428 393 (1981).
1429 [12] R.C. Greenwood *et al.*, Nucl. Instrum. Methods Phys.
1430 Res., Sect. A **390**, 95 (1997).
1431 [13] T. Yoshida *et al.*, *Assessment of Fission Product Decay*
1432 *Data for Decay Heat Calculations*, OECD/NEA Working
1433 Party for International Evaluation Co-operation, Volume
1434 25, 2007.
1435 [14] M. Gupta *et al.*, *Decay Heat Calculations: Assessment*
1436 *of Fission Product Decay Data Requirements for Th/U*
1437 *Fuel*, IAEA report INDC(NDS)-0577, 2010.
1438 [15] A. Algora *et al.*, Phys. Rev. Lett. **105**, 202501 (2010).
1439 [16] RIPL-3, R. Capote *et al.*, Nucl. Data Sheets **110**, 3107
1440 (2009).
1441 [17] M. Fleming and J. C. Sublet, *Decay Data Comparisons*
1442 *for Decay Heat and Inventory Simulations of Fission*
1443 *Events*, UK Atomic Energy Authority, Culham Science
1444 Centre, CCFE-R(15)28/S1, 2015.
1445 [18] C. Bemporad *et al.*, Rev. Mod. Phys. **74**, 297 (2002).
1446 [19] S.-B. Kim *et al.*, Adv. High Energy Phys. **2013**, 453816
1447 (2013).
1448 [20] M. Cribier, Nucl. Phys. B (Proc. Suppl.) **221**, 57 (2011).
1449 [21] K. Schreckenbach *et al.*, Phys. Lett. B **160**, 325 (1985).
1450 [22] A. A. Hahn *et al.*, Phys. Lett. B **218**, 365 (1989).
1451 [23] N. Haag *et al.*, Phys. Rev. Lett. **112**, 122501 (2014).
1452 [24] Th. A. Mueller *et al.*, Phys. Rev. C **83**, 054615 (2011).
1453 [25] P. Huber, Phys. Rev. C **84**, 024617 (2011).
1454 [26] G. Mention *et al.*, Phys. Rev. D **83**, 073006 (2011).
1455 [27] A. C. Hayes *et al.*, Phys. Rev. Lett. **112**, 202501 (2014).
1456 [28] D. L. Fang and B.A. Brown, Phys. Rev. C **91**, 025503
1457 (2015).
1458 [29] M. Fallot *et al.*, Phys. Rev. Lett. **109**, 202504 (2012).
1459 [30] Y. Abe *et al.*, J. High Ener. Phys. **10**, 086 (2014).
1460 [31] J. H. Choi *et al.*, Phys. Rev. Lett. **116**, 211801 (2016).
1461 [32] F. P. An *et al.*, Phys. Rev. Lett. **116**, 061801 (2016).
1462 [33] A. C. Hayes *et al.*, Phys. Rev. D **92**, 033015 (2015).
1463 [34] D. A. Dwyer and T. J. Langford, Phys. Rev. Lett. **114**,
1464 012502 (2015).
1465 [35] A. A. Sonzogni *et al.*, Phys. Rev. C **91**, 011301 (2015).
1466 [36] A. A. Zakari-Issoufou *et al.*, Phys. Rev. Lett. **115**, 102503
1467 (2015).
1468 [37] O. Tengblad *et al.*, Nucl. Phys. A **503**, 136 (1989).
1469 [38] G. Rudstam *et al.*, Atomic Data and Nuclear Data Tables
1470 **45**, 239 (1989).
1471 [39] K.L. Kratz *et al.*, Astron. Astrophys. **125**, 381 (1983).
1472 [40] S. Mughabghab, *Atlas of Neutron Resonances* (Elsevier
1473 Science, 2006).
1474 [41] E.M. Burbidge *et al.*, Rev. Mod. Phys. **29**, 547 (1957).
1475 [42] S. Goriely, Phys. Lett. B **436**, 10 (1998).
1476 [43] R. Surman *et al.*, Phys. Rev. C **64**, 035801 (2001).

- 1477 [44] A. Arcones *et al.*, Phys. Rev. C **83**, 045809 (2011).
1478 [45] T. Rauscher *et al.*, Atom. Data and Nucl. Data Tables
1479 **75**, 1 (2000).
1480 [46] J. E. Escher *et al.*, Rev. Mod. Phys. **84**, 353 (2012).
1481 [47] D.R. Slaughter *et al.*, Phys. Lett. B **38**, 22 (1972).
1482 [48] H. Tovedal *et al.*, Nucl. Phys. A **252**, 253 (1975).
1483 [49] F.M. Nuh *et al.*, Nucl. Phys. A **293**, 410 (1977).
1484 [50] S. Raman *et al.*, Phys. Rev. C **28**, 602 (1983).
1485 [51] F.M. Nuh *et al.*, Phys. Lett. B **53**, 435 (1975).
1486 [52] K.L. Kratz *et al.*, Nucl. Phys. A **317**, 335 (1979).
1487 [53] H. Ohm *et al.*, Z. Phys. A **296**, 23 (1980).
1488 [54] C.J. Bischof *et al.*, Phys. Rev. C **15**, 1047 (1977).
1489 [55] G. D. Alkhazov *et al.*, Leningrad Nuclear Physics Insti-
1490 tute, Preprint 1497 (1989).
1491 [56] J.P. Omtvedt *et al.*, Z.Phys. A **339**, 349 (1991).
1492 [57] H. Yamamoto *et al.*, Phys. Rev. C **26**, 125 (1982).
1493 [58] K.L. Kratz *et al.*, Z. Phys. A **312**, 43 (1983).
1494 [59] S.V. Ilyushkin *et al.*, Phys. Rev. C **80**, 054304 (2009).
1495 [60] S.V. Ilyushkin *et al.*, Phys. Rev. C **83**, 014322 (2011).
1496 [61] B. Jonson *et al.*, Proc. 3rd Int. Conf. on Nuclei far from
1497 stability, CERN Report 76-13 (1976) 277
1498 [62] R. F. Carlton *et al.*, Phys. Rev. C **38**, 1605 (1988).
1499 [63] M. C. Brady, Ph. D. thesis, Texas A&M University, 1989.
1500 [64] ENDF/B-VII.1, M.B. Chadwick *et al.*, Nucl. Data Sheets
1501 **112**, 2887 (2011).
1502 [65] A.-A. Zakari-Issoufou, PhD. Thesis, University of
1503 Nantes, to be published.
1504 [66] I. Moore *et al.*, Nucl. Instrum. Methods Phys. Res., Sect.
1505 B **317**, 208 (2013).
1506 [67] T. Eronen *et al.*, Eur. Phys. J. A **48**, 46 (2012).
1507 [68] S. Agostinelli *et al.*, Nucl. Instrum. Methods Phys. Res.,
1508 Sect. A **506**, 250 (2003).
1509 [69] J. L. Tain *et al.*, Nucl. Instrum. Methods Phys. Res.,
1510 Sect. A **774**, 17 (2015).
1511 [70] D. Cano-Ott *et al.*, Nucl. Instrum. Methods Phys. Res.,
1512 Sect. A **430**, 488 (1999).
1513 [71] J. Agramunt *et al.*, Nucl. Instrum. Methods Phys. Res.,
1514 Sect. A **807**, 69 (2016).
1515 [72] J. L. Tain *et al.*, Nucl. Instrum. Methods Phys. Res.,
1516 Sect. A **571**, 719 (2007).
1517 [73] J. L. Tain *et al.*, Nucl. Instrum. Methods Phys. Res.,
1518 Sect. A **571**, 728 (2007).
1519 [74] D. Cano-Ott *et al.*, Nucl. Instrum. Methods Phys. Res.,
1520 Sect. A **430**, 333 (1999).
1521 [75] S. Goriely *et al.*, Phys. Rev. C **78**, 064307 (2008).
1522 [76] M.-G. Porquet *et al.*, Eur. Phys. J. A **28**, 153 (2006).
1523 [77] J. Genevey *et al.*, Phys. Rev. C **59**, 82 (1999).
1524 [78] See Supplemental Material at *link* for tables of the β in-
1525 tensity distribution from this work.
1526 [79] ENSDF Analysis Programs - LOGFT, National Nu-
1527 clear Data Center, Brookhaven National Laboratory,
1528 http://www.nndc.bnl.gov/nndcscr/ensdf_pgm/analysis/logft/
1529 [80] S. J. Rice, Decay Heat Measurements of Fission Frag-
1530 ments ^{86}Br , ^{91}Rb and ^{94}Sr Using Total Absorption
1531 Gamma-ray Spectroscopy, PhD Thesis, University of
1532 Surrey, 2014 (to be published).
1533 [81] A. J. Koning *et al.*, Journal of the Korean Physical Soci-
1534 ety **59**, 1057 (2011).
1535 [82] D. Jordan *et al.*, Phys. Rev. C **87**, 044318 (2013).
1536 [83] B. C. Rasco *et al.*, Phys. Rev. Lett. **117**, 092501 (2016).
1537 [84] A. J. Koning *et al.*, Proceedings International Conference
1538 on Nuclear Data for Science and Technology, April 22-27,
1539 2007, Nice, France, EDP Sciences (2008) 211.
1540 [85] A. J. Koning *et al.*, Nucl. Phys. A713 (2003) 231
1541 [86] P. Möller *et al.*, Phys. Rev. C **67**, 055802 (2003).